Elastic Light Scattering and Optoelectronic Response of Spherical Silicon Microresonators

by

Ulaş Sabahattin Gökay

A Thesis Submitted to the

Graduate School of Science and Engineering

in Partial Fulfillment of the Requirements for

the Degree of

Doctor of Philosophy

in

Physics

Koc University

Sep 2014

Istanbul

Koc University

Graduate School of Sciences and Engineering

This is to certify that I have examined this copy of a doctor of philosophy's thesis

by

Ulaş Sabahattin Gökay

and have found that it is complete and satisfactory in all respects,

and that any and all revisions required by the final

examining committee have been made.

Committee Members:

_____

Ali Serpengüzel, Ph. D. (Advisor)

_____

Özgür Müstecaplıoğlu, Ph. D.

_____

Şükrü Ekin Kocabaş, Ph. D.

_____

Erdem Alaca, Ph. D.

Date:

Erdal Bulgan, Ph. D.

_____

ABSTRACT

We review the microsphere optical resonators with their whispering gallery modes (WGMs) and the coupling of light to the microspheres by optical fiber half couplers (OFHCs). A theoretical background for the optical resonances in spherical particles is given for plane wave excitation using the Lorenz-Mie Theory, and Gaussian beam excitation using the Generalized Lorenz-Mie Theory (GLMT). Numerical simulations for plane wave excitation using LMT, and Gaussian beam excitation using GLMT are obtained to explain the experimental light scattering results. A brief desription ot the experimental light scattering setup is given together with the properties of the silicon microsphere. The elastic light scattering and the observation of the WGMs on the silicon microspheres are presented for 0° transmission and 90° elastic scattering. The mode structure is analyzed with the mode spacing and quality factor measurements, which corresponds well with the theoretical expectations. The analysis of the WGM spectrum continues with the characterization of the WGM clusters. These clusters can either be explained by the azimuthal mode splitting due to ellipticity or the the mode splitting induced by a particle. The observed assymetrical lineshapes in the spectra are also explained. The presented measurements shows a Fano type lineshape for the 90° elastic light scattering. This line shape is explained by the phase relation of the WGMs with the background created by the surface imperfections and the glare spots. The Fano lineshape observed in the measurements can be used for fast switching and filtering applications. A biosensing scheme for DNA particles is also presented, where a particle adsorbed on the microsphere creates an observable shift in the WGM spectrum. All in all, the optical resonances, namely WGMs are characterized towards possible applications in sizing, sensing and filtering applications. Silicon microsphere is a promising candidate for various novel photonic applications.

ACKNOWLEDGEMENTS

Contents

LIST OF TABLES

LIST OF FIGURES

NOMENCLATURE

OFHC	optical fiber half coupler
WGM	whispering gallery mode
EM	electromagnetic field
FSR	free spectral range
TIR	total internal reflection
b	Impact parameter of a spherical resonator
a	Radius of the spherical resonator
N_{sph}	Refractive index of the spherical resonator
κ, *t*	Inner coupling parameters
κ*, *t**	Outer coupling parameters
b_i, a_i	Complex amplitudes for modes
α	Inner circulation loss coefficient
r	Radial distance
θ	Polar angle
φ	Azimuthal angle
n	Polar mode number
l	Radial mode number
m	Azimuthal mode number
x	Size parameter
λ	Wavelength in vacuum
p	Momentum of a photon in vaccuum
k	Wavevector of a photon in vacuum
$\Delta\lambda_n$	Polar Mode spacing
Q	Quality factor

$N_{i,t}$	Refractive indices of the incident and transmitted media
$\theta_{i,t}$	Interface angles at the incident and transmitted media
$\theta_{brewster}$	Brewster angle at an interface
$\theta_{critical}$	Critical angle at an interface
N_{real}	Real part of the refractive index of the sphere
$N_{imaginary}$	Imaginary part of the refractive index of the sphere
$N_{relative}$	Refractive index of the microresonator relative to outside medium
$\vec{B}$	Magnetic field associated with an EM wave traveling in free space
$\vec{E}$	Electrical field associated with an EM wave traveling in free space
$\vec{D}$	Electrical field of an EM wave traveling in a medium
$\vec{H}$	Magnetic field of an EM wave traveling in a medium
$\vec{J}$	Current density in a medium
ρ	Charge density in a medium
$\vec{\Psi}$	Wave function of a photon
$c(\vec{r})$	Speed of light in direction $\vec{r}$
$f(\vec{r}, t)$	Function defining the physical parameters of the medium
$\vec{E}_{inc}$	Incident electric field
$\vec{E}_{scat}$	Scattered electric field
$\vec{E}_{int}$	Internal electric field
a_v , b_v	the incident field expansion coefficients
c_μ , d_μ	the internal field expansion coefficients
f_v , g_v	the scattered field expansion coefficients
$\overrightarrow{M_v^1}$, $\overrightarrow{N_v^1}$	the spherical harmonic vector functions of the first kind
$\overrightarrow{M_v^3}$, $\overrightarrow{M_v^3}$	the spherical harmonic vector functions of the third kind
ω_o	Half width at the half maximum of the Gaussian beam

L	Orbital angular momentum operator
L_z	Azimuthal part of the orbital angular momentum operator
F	Finesse
$\Delta\lambda_{FWHM}$	Full width at half maximum (linewidth) of a resonance
E_{stored}	Stored energy in a resonator
E_{loss}	Lost energy in a resonator in one cycle
ω	Angular resonance frequency
τ	Lifetime of a photon in a resonance
Q_{total}	Total quality factor of a resonator
$Q_{material}$	Material dependent quality factor
$Q_{s.s}$	Surface scattering dependent quality factor
Q_{cont}	Surface scattering dependent quality factor
Q_{calc}	Calculated quality factor

Chapter 1

Introduction

1.1   Microsphere Resonators

Light and material interactions have become the tools of the modern technology. One of the examples of such interactions is the formation of light resonances in a closed structure. Resonance phenomenon is not a new concept, since the architects have built circular domes, which can contain whispering galleries for sound waves (figure 1.1). Inside these domes, when a person stands close to the circular walls of the dome, he could hear whispers of the people located far across the room [1].

With the starting of the 20th century, whispering gallery modes were analytically explained by Lord Rayleigh [2]. The sound waves produced in a symmetric closed structure can bounce and travel on the walls, while creating sound resonances within the structure and thus becoming contained in the circular gallery. While in resonance, the sound would decay in intensity with the inverse of the distance rather than the inverse square as in the case of a point source of sound radiating in all directions. This accounts for

the whispers being audible all-round the gallery and gives rise to famous architectural wonders.
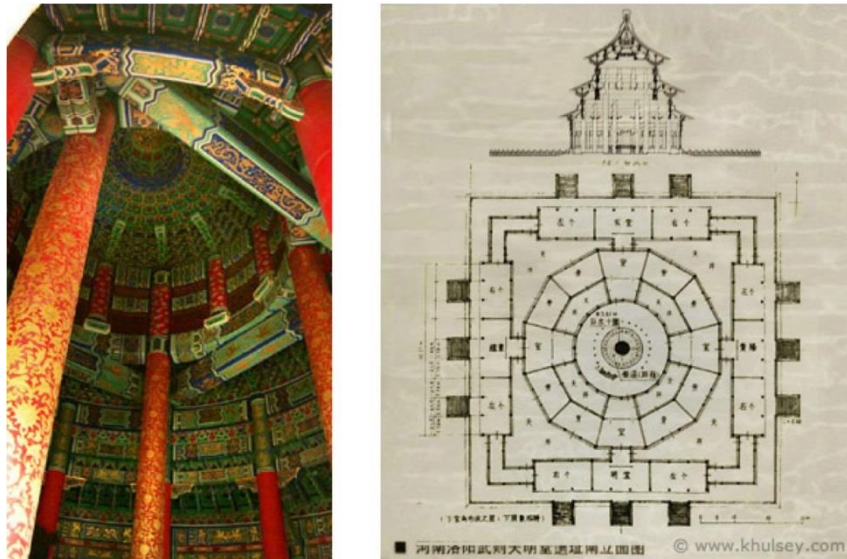
Figure 1.1: Oldest known whispering gallery under the dome of the Temple of Heaven, Beijing, China.

Fitting of sound waves into a circular structure involves the physics of the sound wave resonances, which is based on the constructive wave interference. Much like sound, light waves can also experience constructive interference in a medium and can create optical resonances in a closed structure. When light is incident on a diffractive medium such as a glass sphere, it is refracted into the medium as it passes the boundary between the glass and air. Inside the sphere, light waves can only travel close to the surface due to the total internal reflection (TIR) of the light. Light will reflect back into the sphere from the boundary surface of the glass and will become contained along the surface. Contained light

waves will than go through the constructive wave interference and will show light resonances on the boundary of the medium.

When light resonances are created in a compact and symmetrical medium, the spectra of the light shows high quality factor resonant peaks. These peaks occur due to the narrow linewidth of the whispering gallery modes of the light, which is confined in a small mode volume. Since the resonances have very narrow linewidths, they are also extremely sensitive for the particles in the close vicinity. As a result, highly symmetrical microsized structures can be used for optical detection of the small molecules and particles [3], [4], [5], [6].

Detection of biomolecules has been demonstrated by monitoring the wavelength shifts of the whispering gallery modes (WGMs) due to the binding of the molecules on the resonator surface [7]. However, particle sizing based on the estimation of spectral shifts is slow and is extremely sensitive to the laser intensity and frequency as well as thermal and environmental disruptions. Spectral shifts also depend on the interaction strength between the particle and the WGM, which in turn is effected by the particle location. As a result, small particles with larger overlap can give the same spectral shifts as with the large particles having smaller overlap with the WGM [8].

The solution to this problem is to create particle scattering induced mode splitting, which was previously shown for microspheres [9]. Due to the confinement of the photons in the spherical cavity, Rayleigh scattering of the photons has to be suppressed in high

quality factor whispering gallery modes in microspheres. These modes are created by the traveling of photons around the rim and can be in clockwise and counter clockwise direction depending on the splitting. Formulation of the modes can be explained by spherical Bessel and Hankel functions and the properties of the light in this state can be sensitively calculated. Early estimations for the limit of the quality factor are $Q \approx 10^{10}$ for the fused silica spheres, but the resonance condition is extremely sensitive to the surface hydration and contamination of the spheres [10]. This extreme sensitivity is useful for detecting particles with radius of 40-50 nm but smaller particles were a challenge because the measurement becomes noise heavy. Using microspheres is beneficial for average size particle detection such as dust, but for biomedical applications high noise level has to be solved together with the particle identification [11].

1.2   Coupling of light to the microsphere resonators

Analytic theory of coupling from tapered fibers and optical fiber half couplers (OFHC) into the microsphere resonators involves the solution of the characteristic equation for the light mode [12]. Since the optical resonator is a microsphere, Bessel and Hankel functions in spherical geometry are used for the characteristic equation. The characteristic equation relates the spherical mode orders to the resonant light mode in the sphere, where the equatorial plane is defined as the circle, along which the modes are most strongly coupled. A light mode in a sphere is defined by spherical mode numbers (*l, n, m*). The

number of field maxima in the radial direction is given by l, while the number of field maxima in polar direction is n with azimuthal mode numbers of m. The incoming light brought to the close vicinity of the sphere with various coupling methods are described below and the optical trapping of photons on the surface of the resonator occurs due to the total internal reflection (TIR).

The coupling of light to the microresonators can be listed as angle polished tips [13], planar waveguides [14], optical fiber half coupler (OFHC) [4] and tapering of the fiber core [15], [11], [16]. Using OFHC method for the coupling of evanescent Gaussian beams to the WGMs in microspheres is more favorable due to the creation of smaller optical mode volumes thus becoming critically coupled [17], [18], [19].

The coupling of WGMs by plane or Gaussian waves focused on the equatorial rim of a microsphere is not efficient due to the small scattering cross section for the interaction [20], [21]. Although useful for optical pumping mechanisms, this method might lead to the weak trapping of photons and might hinder the formation of WGMs.

Since the overall interaction is energy exchange between the photons and the geometrical shape, it is more preferable to use guided light modes with evanescent field tails, [22], [23]. Since an overlap of the fields is required, prism coupling [24] became the widely used coupling configuration and has been adapted by angle polished optical fibers tips [13].

Optical fiber half couplers (OFHC) yield the original optical mode to have a great disturbance over the fiber core, where at the outside of the fiber core and the OFHC, the field decays with an evanescent field tail. Generally the fibers with larger core diameter can carry more confined modes but couple weakly to the spheres. Half block couplers has a larger spot size near the polished surface so the waveguide and the sphere are more efficiently coupled in the fundamental mode ($m \approx n$), whereas azimuthal mode orders require tapered fiber. Light in the polished half block waveguide has a broad transverse field, which is matched in spatial extent to the fundamental sphere mode by bringing the sphere to the close proximity of the waveguide [12].

Chapter 2

Theory of the Whispering Gallery Mode Resonators

This chapter includes a general theory of the light resonance in spherically symmetric light resonators. Light is first studied in geometrical optics with Snell's law of refraction, while total internal reflection (TIR) and the resonance condition of the light are explained. Plane wave representations of the light are used to explain the polarization dependence of the light in Fresnel's equations and this helps building of the basic resonator theory by defining the size parameter (x). As the wavelength of the light (λ) becomes much smaller than the size of the resonator, Mie scattering becomes dominant for the explanation of the behavior of the light, so vectorial harmonic spherical modes of the light are introduced. Modal structure of the light inside a spherical resonator leads to specific mode families and individual resonant modes in the scattering spectra of the resonator and fundamental parameters such as free spectral range (FSR), polar mode spacing ($\Delta\lambda_n$) and quality factor (Q) can be expressed. Among these parameters quality factor determines the losses in the resonance and will be presented in terms of the loss mechanisms. After this step, a section for light coupling to the microspheres will be given. This section includes the universal coupling equations and will be followed by the optical fiber half coupler (OFHC) with

evanescent wave coupling mechanisms. Overall, this chapter is intended to establish a theoretical background for the evanescent wave coupling to a spherical resonator.

2.1   Geometrical Representation of the Light at a Dielectric Interface

Snell's law describes the light moving from a medium with refractive index of N_i to a medium with refractive index N_t with a relation between the angles of the rays and the refractive indices of the both media:

$$N_i \sin \theta_i = N_t \sin \theta_t \tag{2.1}.$$

The above relation can also be used to describe the geometrical light ray as a wave, which refracts and reflects when encountering a boundary between two media. A wave of light can also be understood with its counterpart, photon, so that electric and magnetic fields associate to a photon traveling at the speed of light c. Understanding the light as a wave takes place in Fresnel equations, where the direction of the electrical field defines the polarization of the field. If the transverse directional fields are continuous through the boundary, then the reflection (r) and transmission (t) coefficients of the electric fields of light can be obtained for TE and TM polarizations [25]:

$$r_{TE} = \frac{N_i \cos(\theta_i) - N_t \cos(\theta_t)}{N_i \cos(\theta_i) + N_t \cos(\theta_t)}, t_{TE} = \frac{2N_i \cos(\theta_i)}{N_i \cos(\theta_i) + N_t \cos(\theta_t)} \tag{2.2},$$

$$r_{TM} = \frac{N_i \cos(\theta_t) - N_t \cos(\theta_i)}{N_i \cos(\theta_t) + N_t \cos(\theta_i)}, t_{TM} = \frac{2N_i \cos(\theta_i)}{N_i \cos(\theta_t) + N_t \cos(\theta_i)} \tag{2.3}.$$
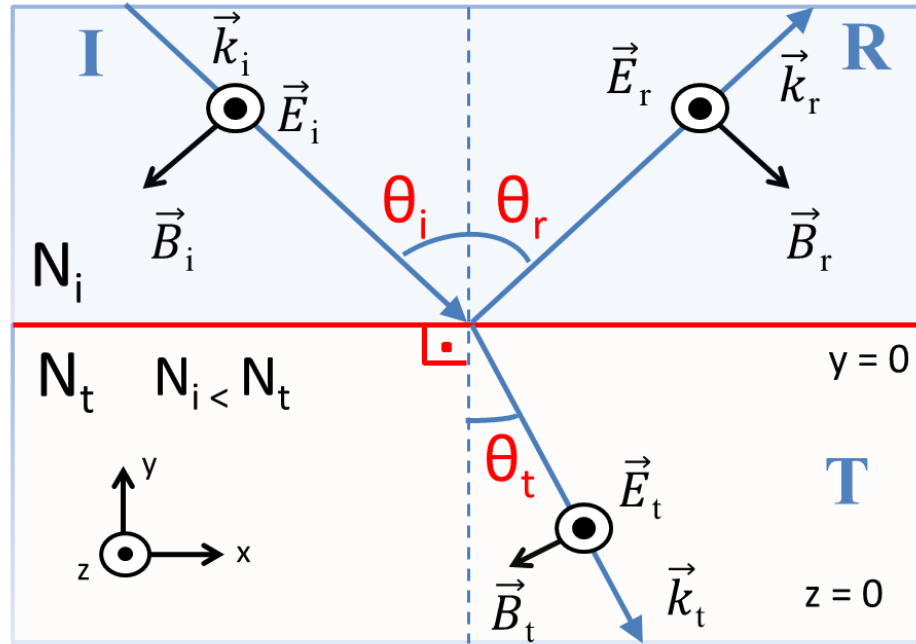
Figure 2.1: Reflection and refraction of the light with TE polarization.

When light encounters a boundary, it can refract and reflect simultaneously. Rates of passing through or being reflected depends on the polarization of the light field and the angle of the incidence. Together with Fresnel and Snell equations, it can be seen that, depending on the refractive indices of the two media, there is a critical angle for zero reflection of the incident light:

$$\theta_{Brewster} = \arctan(N_t/N_i) \tag{2.4.}$$
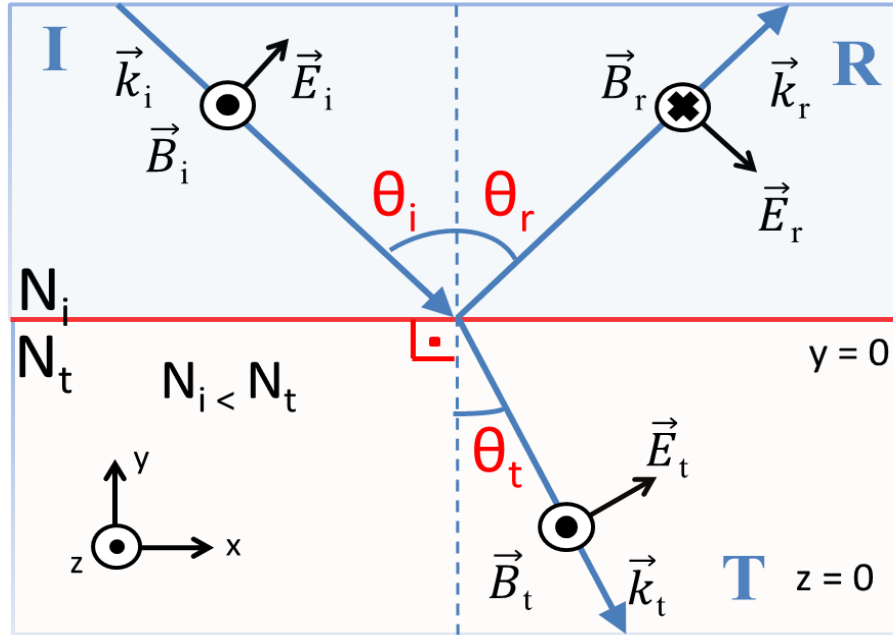
Figure 2.2: Reflection and refraction of light with TM polarization

2.2   Total Internal Reflection at a Dielectric Interface

If the light is incident from a higher index medium to a lower index medium ($N_i > N_t$) than after a critical angle of:

$$\theta_{critical} = \arcsin(\frac{N_t}{N_i}) \tag{2.5}$$

total internal reflection (TIR) can be observed.
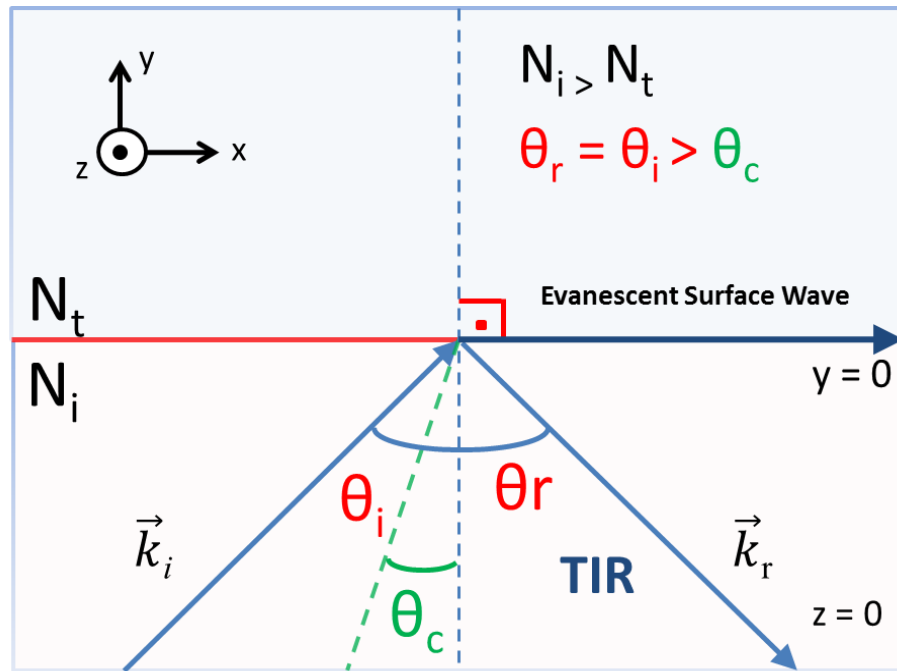
Figure 2.3: Total internal reflection of light.

The evanescent surface waves are near field waves with an intensity that has an exponential decay into the outside low index medium [26], [27]. The evanescent waves can travel on the boundary of the two refractive media with different optical properties. The geometrical picture for the total internal reflection (TIR) with the incidence and reflectance angles may not be enough for the explanation of the evanescent waves; the model predicts the TIR light traveling on the boundary due to the incoming light having angles equal or greater than the critical angle, but the explanation for the evanescent waves comes from the solution of Maxwell's equations [28].

Evanescent waves present many applications in the fields of optics and photonics. A well known application of the evanescent fields is in the field of spectroscopy [29], [30]. Apart from these, sensing of the small objects such as molecules and proteins with the help of evanescent fields are also known [31], [32]. Among these applications, the use of evanescent waves produced by the elastic scattering of the light in a silicon sphere are the most suitable for the aim of detection and sensing [33].

2.3   Optical Resonances in Circular Cavities

In this section, the basics of the WGMs excited in the spherical dielectric particles will be presented. Geometrical picture of the optical resonances state that, when light rays propagate through the boundary surface of a spherical medium, they refract and hit the surface of the medium with an angle of incidence of θ_i, and if $\theta_i \geq \theta_{critical} = \arcsin(1/N_{sphere})$, then total internal reflection (TIR) occurs (fig. 2.3). Light rays reflect along the equatorial rim of the spherical structure with identical subsequent reflected angles thus propagate close to the surface (fig. 2.4).

The description of the optical resonances in microspheres is based on the Fabry-Perot etalons, where the spherical boundary of the medium replaces the etalon mirrors and the optical path length is the circumference of the sphere. In this case, resonance condition of the light in a microsphere can be presented in relatively simple terms, if the wave picture of the light is used. For the case of a microsphere with circumference much larger than the

wavelength of the light ($2\pi a \gg \lambda$), and light rays having near glancing incidence angles of $\theta_i \approx 90^o$, the optical path length for the light rays traveling inside the microsphere in a single round-trip should be approximately equal to the circumference of the sphere as;

$$n\lambda = N_{sphere}2\pi a \qquad (2.6),$$

where N_{sphere} is the refractive index of the microsphere and n an integer. Since the optical resonances are distributed along the circumference of the microsphere, the resonance condition is related to the size parameter;

$$x = \frac{2\pi a N_{outside}}{\lambda} \qquad (2.7).$$
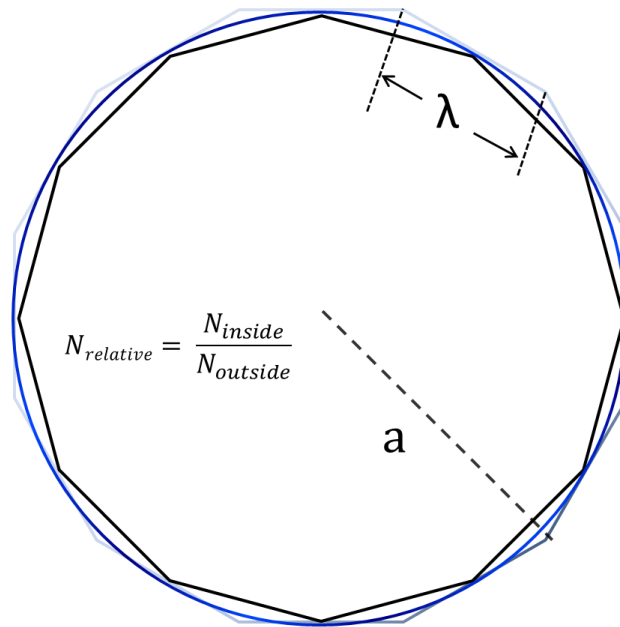
Figure 2.4: Schematic for WGM in a spherical resonator.

Equation 2.6 describes the standing wave condition on the microsphere, where the integer number n describes the number of intensity maxima distributed along the circumference. The limits of n depend on the optical path length for one roundtrip of light, which is mostly confined within the microsphere and extends shortly into the surrounding medium. This relation can be presented by using the size parameter (x) of the sphere:

$$x \leq n \leq x N_{sphere} \qquad\qquad (2.8).$$

The above equation will also be used in the coupling of light to the microsphere. Geometric optics helps explaining of the WGMs in a spherical particle, however for a perfect sphere, light rays traveling close to the surface of the sphere should not leak out due to the condition of $\theta_i \geq \theta_{critical}$. In this case, light rays would be completely confined in the sphere and WGMs would not be visible for an outside observer. This question can be answered with the field representations of light in the microsphere, where diffraction of the waves due to the curvature of the sphere causes light to leak out tangentially from the equatorial rim.

2.4   Field representations of light in a medium

The light consists of photons, which have associated electric and magnetic fields traveling with the speed of light in vacuum. When photons are traveling inside a medium,

they also carry associated fields, but this time electrical and magnetic fields are converted into displacement fields. Behavior of the light propagating in a medium can be given by the Maxwell equations as follows [34]:

$$\frac{\partial \vec{B}}{\partial t} + \vec{\nabla} \times \vec{E} = 0$$

$$\frac{\partial \vec{D}}{\partial t} - \vec{\nabla} \times \vec{H} = \vec{J}$$

$$\vec{\nabla} \cdot \vec{D} = \rho$$

$$\vec{\nabla} \cdot \vec{B} = 0 \tag{2.8}.$$

When a photon encounters a boundary between two media the wavefunction of the photon goes through a transformation, which depends on the refractive indices of the media and the geometry of the boundary between them. In order to analytically define the fields in various geometries, mathematicians studied membranes in square, circle and spherical surfaces and produced coordinate representations of the wave equation:

$$\vec{\Psi} - \frac{1}{c^2(\vec{r})} \frac{\partial^2}{\partial t^2} = f(\vec{r}, t) \tag{2.9},$$

where $\vec{\Psi}$ is the wave function, $c(\vec{r})$ is the speed of light in direction $\vec{r}$ and $f(\vec{r}, t)$ is a function defining the physical parameters of the medium. When $f(\vec{r}, t)=0$ then the wave equation reduces to the Helmholtz equation, which yields to an electromagnetic wave traveling in vacuum. If the wavelength of the light is less than the radius of the resonator medium, then this interaction can be explained by the Lorenz-Mie theory [35], [36].

2.4.1   Lorenz-Mie Theory

The interaction of light with homogenous and geometrical dielectric media can be explained by expanding the electric and magnetic fields of the light into vectorial harmonic functions as the solutions of the Helmholtz equation [37]. In the case of spherical particles, whose diameter is much larger than the wavelength of the light, electromagnetic fields can be expressed as a combination of vectorial spherical harmonic functions with the convenience of the spherical coordinate representations. These functions contain expansion coefficients, which constitute the intensity of the scattered fields inside and outside of the sphere. Together with the polarization of the fields, expansion coefficients can be given as [38];

$$a_n = \frac{j_n(x)[N_r x j_n(N_r x)]' - N_r^2 j_n(N_r x)[x j_n(x)]'}{h_n^{(2)}(x)[N_r x j_n(N_r x)]' - N_r^2 j_n(N_r x)[x h_n^{(2)}(x)]'} \qquad (2.10),$$

$$b_n = \frac{j_n(x)[N_r x j_n(N_r x)]' - j_n(N_r x)[x j_n(x)]'}{h_n^{(2)}(x)[N_r x j_n(N_r x)]' - j_n(N_r x)[x h_n^{(2)}(x)]'} \qquad (2.11).$$

The above equations contain spherical Bessel functions $j_n(x)$ and Hankel function of the second kind $h_n^{(2)}(x)$ with the derivative with respect to the argument is donated with a prime. Functions are defined on the size parameter x while $N_{relative}$ is the relative refractive index of the sphere with respect to the outside medium. The coefficients for the internal and external fields are identical for both polarizations, whereas zeros of the denominators correspond to the whispering gallery modes (WGMs) of the microsphere [39].

The mode of the light in a microsphere can be expressed with mode numbers (*l, n, m*), which characterize the radial, polar and azimuthal components of the electromagnetic field in a microsphere. Radial mode number *l* (*l* = 1,2,3 …) gives the number of maxima in the radial part of the field distribution, whereas polar (angular) mode number *n* (*n* = 0,1,2 …) defines the field intensity distribution in the polar direction. The mode number *m* denotes the azimuthal distribution of the field and is degenerate with 2*n*+1 values (*m* = -*n*,-*n*+1 ..., 0, …, *n*-1,+*n*). This degeneracy can be removed by making the sphere deformed to have an oblate or prolate shape. Mode numbers for the description of the light inside the spherical resonator arise naturally with the solution of the characteristic equation together with the solution of the resonance condition (Eqn. 2.6).

Parameter / Function	Symbol	Values
Radial mode (Legendre)	l	1,2,3,…
Polar (angular) mode (Bessel)	n	0,1,2,…
Azimuthal (equatorial) mode (Bessel)	m	$-n \leq m \leq +n$, ($2n+1$ values)

Table 2.1. Parameter symbols and values for the mode of light trapped in a sphere

The mode numbers for the light resonating in the outer surface of a microresonator can also describe the momentum properties of the photon. The mode number n indicates the order of the spherical harmonic $Y_{n,m}$ and describes the polar angular field distribution, while being the eigenfunction of the square of the orbital momentum operator L:

$$L^2 Y_{n,m} = 2\hbar n(n+1)Y_{n,m} \qquad (2.12).$$

The azimuthal mode number m arises from the projection of the angular momentum on the azimuthal axis and can take $2n+1$ values:

$$L_z Y_{n,m} = m\hbar Y_{n,m} \qquad (2.13).$$

2.4.2 Free Spectral Range, Mode Spacing and Quality Factor

The main properties of the whispering gallery mode (WGM) spectrum are analogous to Fabry-Perot interferometer [40]. For a Fabry-Perot type resonator, wavelength separation between successive polar modes n and $n+1$ on the intensity spectra is called the free spectral range (FSR) as:

$$\text{FSR} = \lambda_n - \lambda_{n+1} \tag{2.15},$$

where $\lambda_{l,n,m}$ is the frequency of a particular mode [41]. When the Fabry-Perot geometry is adjusted for the spherical resonator, Fabry-Perot like FSR of the resonator can be given as:

$$\text{FSR} = \frac{\lambda^2}{2\pi a N_{sphere}} \tag{2.16}.$$

Naturally, the above formula doesn't include the scattering effects induced by the sphere geometry on the WGM resonances. These effects arise from the size parameter (x) of the sphere and the number of polar modes (n). If the limiting case for the resonance parameters; $x \gg 1$, $n \gg 1$, and $x/n \sim 1$, is used with the Lorenz-Mie scattering, the asymptotic formula for the mode spacing of the optical resonances in a microsphere would be [42];

$$\Delta\lambda_n = \frac{\lambda^2 \tan^{-1}\sqrt{N_{rel}^2-1}}{2\pi a N_{outside}\sqrt{N_{rel}^2-1}}$$ (2.17).

The above equation gives the approximate spacing in wavelengths between the two resonances with the same radial mode order l. This spacing is also called as the intra-mode spacing due to the fact that it defines the spectral separation of the resonant modes for the constant polarization of the light. The finesse (F) defines the quality of the individual resonances by relating the FSR with the full-width-at-half-maximum (FWHM) of the resonances:

$$F = \frac{FSR}{\Delta\lambda_{FWHM}}$$ (2.18).

The finesse is a basis for the quality factor definition of the optical resonances in a microsphere. As it is described by the figure 2.5, the linewidth of the resonances are $\delta\lambda$ and the resonance occurs at a wavelength of λ, which yields to a quality factor relation similar to the finesse, as;

$$Q = \frac{\lambda}{\delta\lambda}$$ (2.19).

The quality factor (Q) quantifies the ability to store light and it is a measure of energy losses. Quality factor is also related to the finesse (F) of the resonator and defines the time averaged energy density per the energy loss for a resonant mode in the cavity in one round trip time [43];

$$Q = \omega \times \frac{E_{stored}}{E_{loss}} \qquad (2.20),$$

where ω denotes the angular resonance frequency of the photon. The quality factor defines

the decay time (τ) of that photon during the resonance as;

$$Q = \frac{\omega}{\Delta\omega} = \omega\tau \qquad (2.21).$$
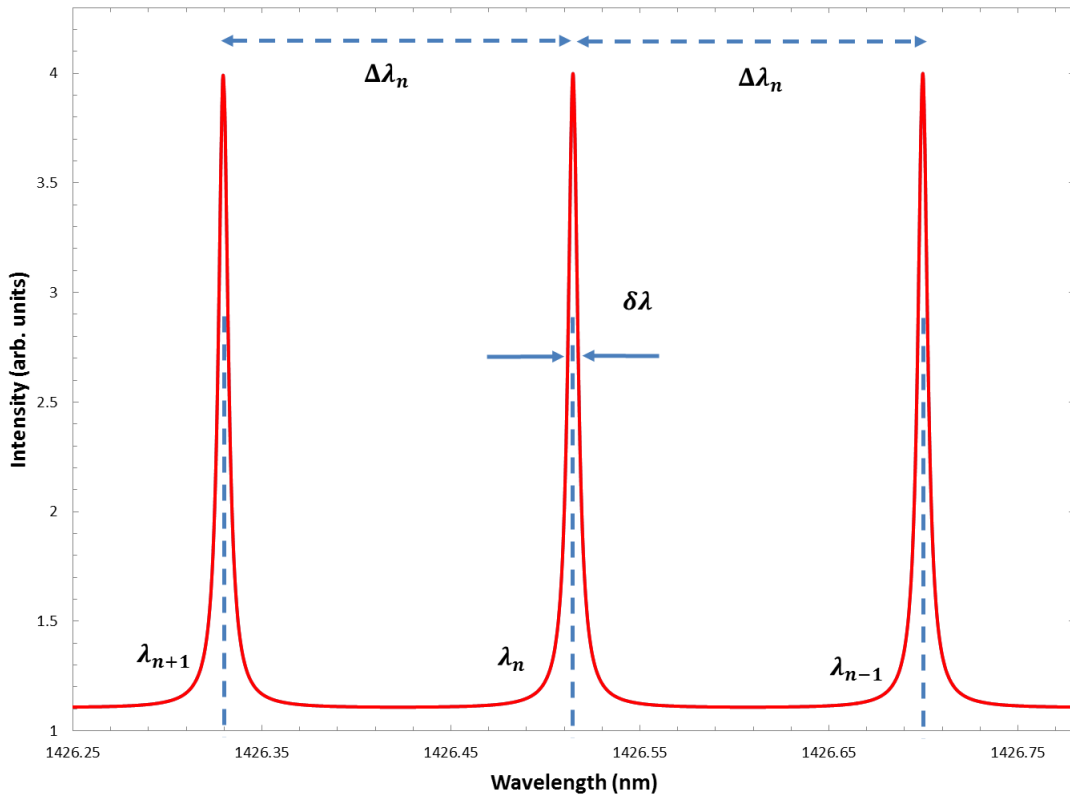
Figure 2.5: Spectral properties of the optical resonances.

The imaginary part of the eigenvalue of the wave number (k) with a resonance determines the decay of the radiation reflected from a curved surface. The radiation scattered from the curved boundary surface of the cavity and the outside medium will decay from the spherical structure with a radiative quality factor [44]. Normally, the quality factor of the bare resonator (Q_{un}) gets into account, when the sphere mode is excited with light, but the contaminants (Q_{cont}) and the surface scattering ($Q_{s.s}$) create the excess energy losses in the power spectra. Overall, the quality factor can be written as a summation over all losses;

$$Q_{total}^{-1} = Q_{un}^{-1} + Q_{s.s}^{-1} + Q_{cont}^{-1} + \cdots \tag{2.22}.$$

2.5   Coupling of Light to the Circular Resonators

2.5.1   Universal Coupling Equations

Spherically symmetric microresonators can interact with light, as can be seen in Fig. 2.5. The light in a waveguide gets transmitted to the resonator through evanescent coupling with coupling coefficients of κ and t, while leading to circulation of light along the circumference. Equations for universal coupling of light between a waveguide and arbitrary resonator geometry can be given by creating a uniform interaction matrix [45]. If a single unidirectional mode of the resonator is excited for a lossless coupling the interaction matrix can be written as:

$$\begin{vmatrix} b_1 \\ b_2 \end{vmatrix} = \begin{vmatrix} t & \kappa \\ -\kappa^* & t^* \end{vmatrix} \begin{vmatrix} a_1 \\ a_2 \end{vmatrix} \qquad (2.23),$$

where b_i and a_i are complex amplitudes of the light modes and κ, t and κ^*, t^* are inner and outer coupling parameters, respectively. Amplitudes of the modes are normalized such that the coupling parameters can be written as $|\kappa^2| + |t^2| = 1$. If the input amplitude is set to be unity (a_1=1), then the transmission around the resonator is given by $a_2 = \alpha e^{i\theta} b_2$ with the inner circulation loss factor of α. Depending on the coupling parameters, the transmission past the resonator on the waveguide can be written as;

$$|b_1|^2 = \frac{\alpha^2 + |t|^2 - 2\alpha|t|\cos(\theta + \phi_t)}{1 + \alpha^2|t|^2 - 2\alpha|t|\cos(\theta + \phi_t)} \qquad (2.24),$$

where $t = |t|exp(i\phi_t)$. The total circulating optical power around the resonator can be given as;

$$|a_2|^2 = \frac{\alpha^2(1 - |t|^2)}{1 - 2\alpha|t|\cos(\theta + \phi_t) + \alpha^2|t|^2} \qquad (2.25).$$

The resonance condition occurs at $(\theta + \phi_t) = n2\pi$, where $n = 0,1,2\dots$ is the mode number in the polar angular direction. The resonance of light in the structure modifies the above equations as;

$$|b_1^2| = \frac{(\alpha - |t|)^2}{(1 - \alpha|t|)^2} \text{ and } |a_2|^2 = \frac{\alpha^2(1 - |t|)^2}{(1 - \alpha|t|)^2} \qquad (2.26),$$

when $\alpha = |t|$ internal losses become equal to the coupling losses, while the transmitted power ($|b_1|^2 = 0$) vanishes so that the critical coupling condition is reached. The outgoing

wave in the waveguide destructively interferes with the circulating internal field and a transmission minimum is seen.
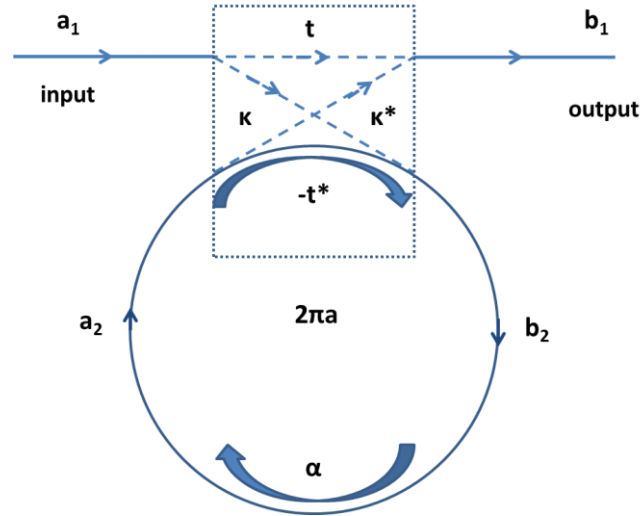
Figure 2.6: Universal scheme for the waveguide coupled to a ring resonator.

2.5.2   Excitation of optical resonances in microspheres

The whispering gallery modes (WGMs) of light in a microsphere requires an excitation mechanism. The laser light should be incident on the microsphere and refract into the sphere to create localization of photons onto the interior surface of the microsphere. In this case, the nature of the incident light is important, i.e., plane wave [46] or Gaussian wave [47] should be used for the excitation of the fields inside and outside of the sphere. Both of the field representations are used to calculate the Mie scattering coefficients for the interaction with a microsphere.

The light coupling to a resonator involves certain matching conditions. These conditions include the distance of the cavity to the excitation source, refractive indices of the media and the phase matching of the input light with the resonator [12]. Excitation of the WGMs in a resonator depends on the relative distances of the cavity center and the beam waist of the excitation source. This distance is called as the impact parameter (b), where the equation 2.8 gives a similar definition over the size parameter (x). The impact parameter defines the efficiency of the coupled resonances inside the resonator medium. In order to maximize the coupling to the cavity, the impact parameter should be limited by the radius of the spherical resonator (a) and with the relative refractive index (N_{rel}):

$$a \leq b \leq aN_{rel} \qquad\qquad (2.27).$$

The overall resonance condition is to excite the cavity modes with the input light by a coupling mechanism, which delivers the light to the close proximity of the cavity in various ways (figure 2.7). Special attention goes to the optical fiber half coupler (OFHC) for the coupling of the light to the microsphere. OFHC consists of a single mode optical fiber (SMOF) buried into a glass block. SMOF is capable of transmitting near infrared light with wavelength of 1550 nm, while having a core refractive index of 1.47 and a cladding refractive index of 1.45. The middle part of the SMOF is polished down to the core (~1-2 μm). The exposed part of the fiber creates an evanescent field tail over the surface, which

can interact with a microsphere positioned to the close proximity. Side and end viewed diagrams for the light coupling with an OFHC can be seen at Fig. 2.8 and Fig. 2.9.

(a)   (b)

(c)   (d)
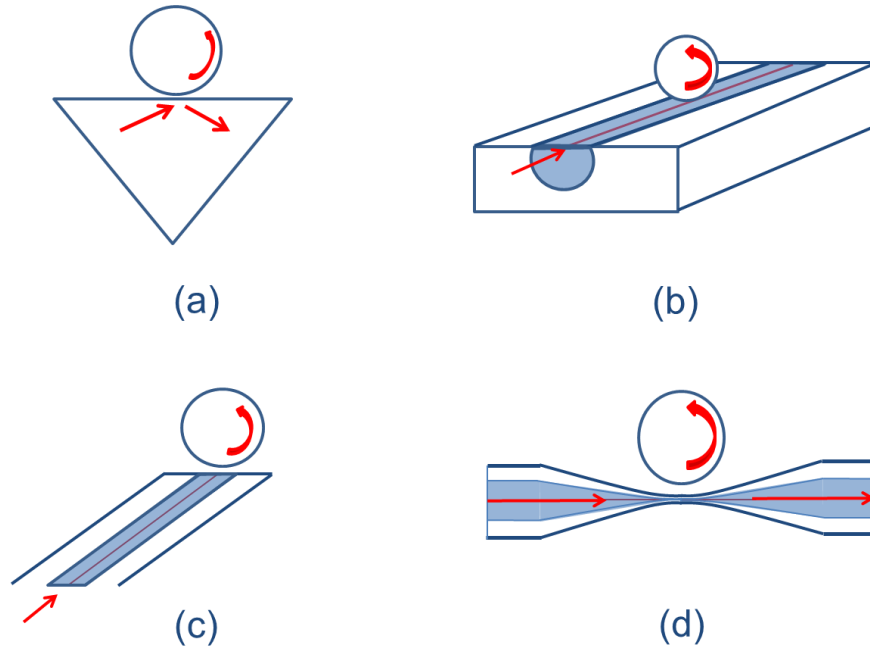
Figure 2.7: Light coupling methods for exciting WGMs in a spherical microresonator, (a) prism, (b) optical fiber half coupler (OFHC), (c) fiber tip, (d) tapered fiber.

Figure 2.8 shows a diagram for the light coupling to a microsphere with OFHC, where a is the radius of the sphere, b the impact parameter, N_{air} and N_{sphere} the refractive indices of the air and the sphere, and the $\vec{k}$ the wavevector of the light traveling through the fiber on the OFHC. Together with the figure 2.9, evanescent field tail of the light can be seen, where the fiber core ($2\omega_0$) defines full-width at half maximum (FWHM) of the Gaussian beam.
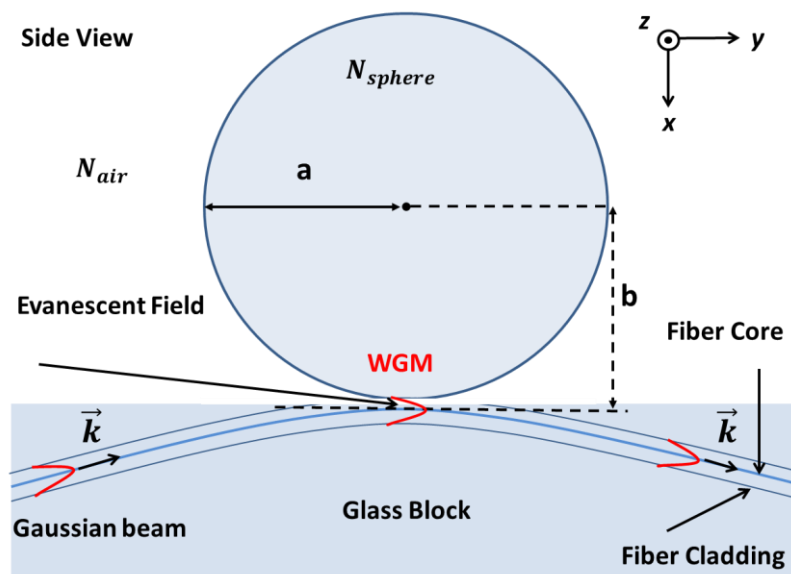
Figure 2.8: Side view of OFHC with the microsphere
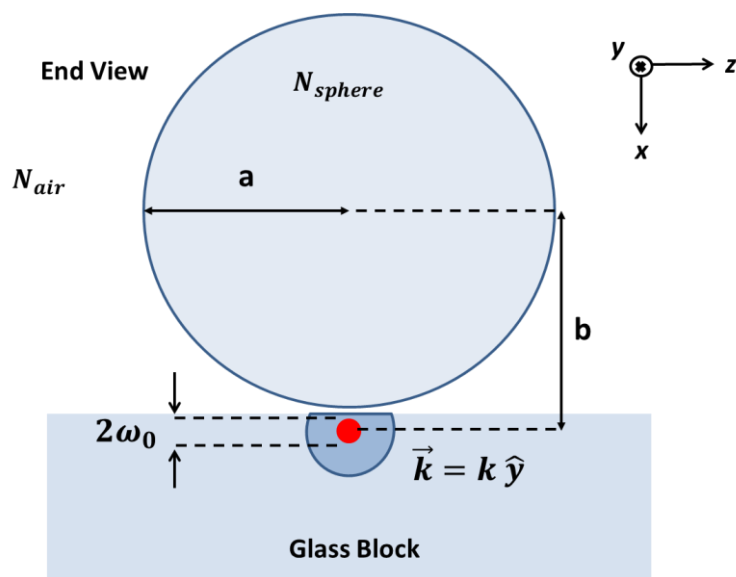
Figure 2.9: End view of the OFHC with respect to the microsphere.

Chapter 3

Numerical Simulation and Analysis of Elastic Scattering in Silicon Microspheres

This chapter summarizes the computational studies of the elastic light scattering by silicon microspheres with plane wave and Gaussian beam excitation. Plane wave excitation results are prepared with implementing the Fortran 77 software prepared by Steven C. Hill and Peter W. Barber with their book titled as 'Light scattering by particles: Computational Methods' [46]. Gaussian beam excitation simulations are performed with the code by James A. Lock [48].

3.1   Plane wave excitation simulations in silicon microspheres

These simulations are carried out in order to obtain the scattered field intensities as a function of wavelength for the determination of the resonant light structure of a silicon microsphere. In order to cover the experimental results, incident field can have parallel ($\parallel$) and ($\perp$) polarization states, whereas the scattered field is observed from polar angles of 0° to 180°. The calculated resonance spectra will be of use for the understanding of the experimental results and the analysis of the light resonances.

3.1.1   Transfer matrix method for the spherical harmonic fields

The light scattering by a small particle can be described by the Lorenz- Mie theory [35], [36]. If the electrical field of the incident light can be expanded in turns of spherical vectorial harmonic functions, than scattered and internal light distributions can be calculated by finding the expansion coefficients [49]. The fields can be calculated with the separation of variables for finding the light intensities over the spherical coordinates. The light distribution is formulated by expanding incident ($\vec{E}_{inc}$), scattered ($\vec{E}_{scat}$) and internal ($\vec{E}_{int}$) electrical fields in terms of spherical harmonic vector functions as [46]:

$$\overrightarrow{E}_{inc}(k\vec{r}) = E_0 \sum_{v=1}^{inf} D_v [a_v \overrightarrow{M_v^1}(k\vec{r}) + b_v \overrightarrow{N_v^1}(k\vec{r})] \tag{3.1},$$

$$\overrightarrow{E}_{scat}(k\vec{r}) = E_0 \sum_{v=1}^{inf} D_v [f_v \overrightarrow{M_v^3}(k\vec{r}) + g_v \overrightarrow{N_v^3}(k\vec{r})] \tag{3.2},$$

$$\overrightarrow{E}_{int}(N_{rel}k\vec{r}) = E_0 \sum_{\mu=1}^{inf} [c_\mu \overrightarrow{M_\mu^1}(N_{rel}k\vec{r}) + d_\mu \overrightarrow{N_\mu^1}(N_{rel}k\vec{r})] \tag{3.3},$$

where $k = \frac{2\pi}{\lambda}$ is the wave vector and N_{rel} the relative refractive index. Other parameters can be listed as; ($v = \sigma, m, n$) and ($\mu = \sigma', m', n'$) the spherical harmonic triple indices, D_v the normalization factor, a_v and b_v the incident field expansion coefficients, c_μ and d_μ the internal field expansion coefficients, f_v and g_v the scattered field expansion coefficients, $\overrightarrow{M_v^1}$ and $\overrightarrow{N_v^1}$ the spherical harmonic vector functions of the first kind, $\overrightarrow{M_v^3}$ and $\overrightarrow{M_v^3}$ the spherical

harmonic vector functions of the third kind. The software utilizes a set of matrix equations to solve the expansion coefficients of the fields simultaneously. By using the expansion coefficients, the field intensity distributions and scattering cross sections for parallel and perpendicular field polarizations can be calculated from 0° to 180°. Schematic of the incident, internal and scattered fields can be seen in figure 3.1.

The array dimensions of the matrices define the maximum size parameter of the spherical particle. If the particle is too large, the convergence of the calculations exceeds the limits. Convergence factor (n_c) of the matrices can be related with the size parameter (x) as:

$$n_c = x + 4.05\, x^{1/3} + 2 \qquad (3.4).$$

The convergence factor also determines the resolution for the wavelength in the light scattering spectra. In order to observe narrow linewidth WGMs in the scattering spectra, the convergence factor must exceed the size parameter as:

$$n_c \geq |N_{rel} x| \qquad (3.5).$$

For a silicon sphere of radius 500 μm, refractive index of the sphere 3.5 and incident wavelength range of 1426 nm – 1427 nm, the size parameter of the resonator is around 2200. This yields to a convergence factor of n_c ~2300. In order to be able to observe WGM spectral lines, the convergence factor should be larger than 7000 and has been modified accordingly. For having sufficient wavelength resolution, the number of data points in all of the simulations is set to be 10^4, which gives a resolution of 0.0002 nm.
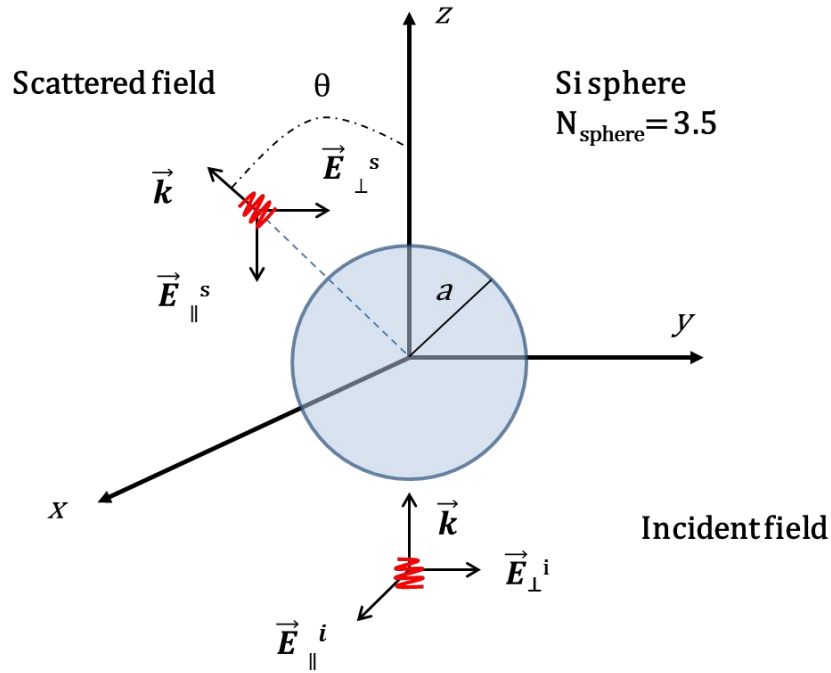
Figure 3.1: Schematic for the geometry of the numerical calculations [46].

3.1.2   Polar Angle dependence of the resonances in the intensity spectra

The polar angle dependence of the elastic light scattering in silicon spheres is calculated for parallel and perpendicular polarization states. A silicon sphere of refractive index 3.5 and radius 500 μm is used for the calculations for the scattering angles ranging from 0° to 180° with 10° steps. The results can be seen in fig. 3.2 for parallel polarization and fig. 3.3 for perpendicular polarization, respectively. The calculated mode spacing on the graphs for each of the polarizations are displayed as gray and white regions to aid the eye.
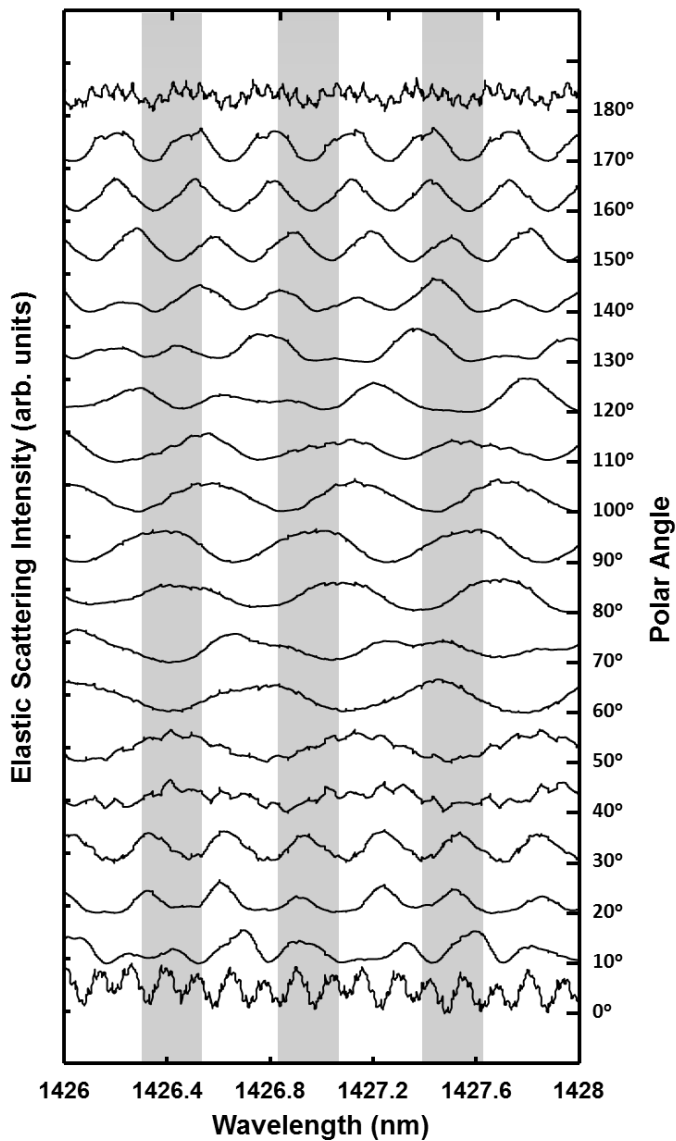
Figure 3.2: Light scattering intensities with parallel polarization calculated for angles from 0° to 180°.
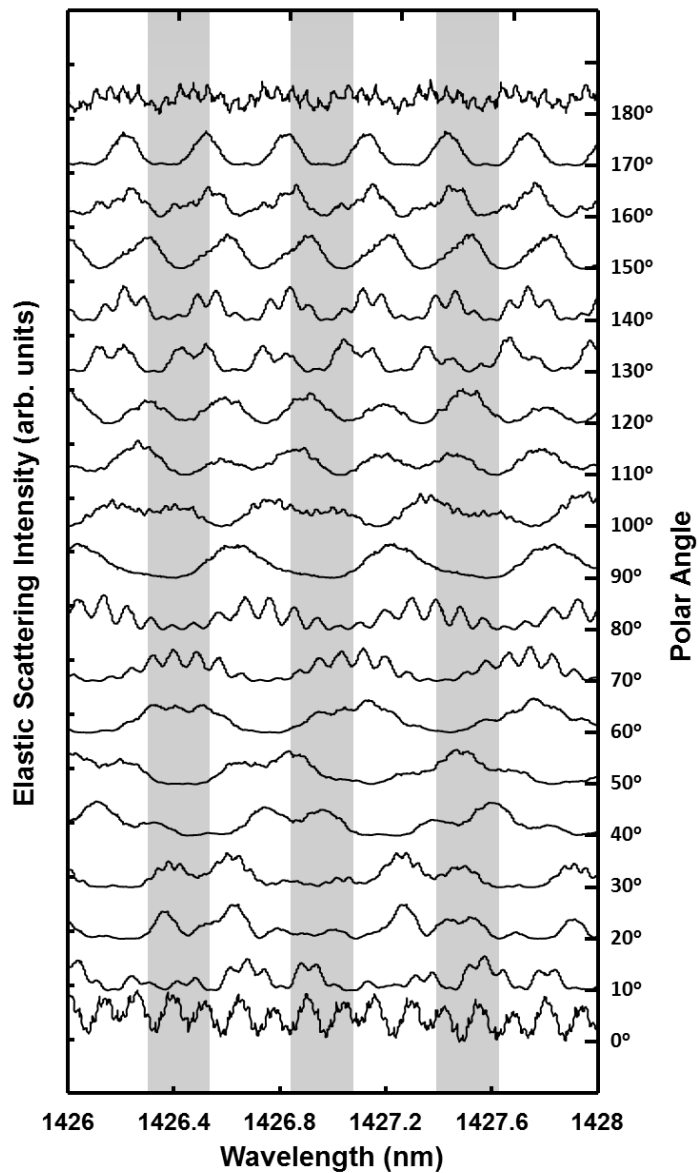
Figure 3.3: Light scattering intensities with perpendicular polarization calculated for angles from 0° to 180°.

The angle variation of the elastic light scattering simulations shows the polar angle dependence of the resonances [50]. For a given polarization, the calculated mode spacing is $\Delta\lambda_n = 0.24$ nm, which is indicated by the gray and white regions in the spectra, where among these angles, different amount of mode families per a mode spacing can be observed. In the parallel polarization, the 0° elastic light scattering (forward scattering) shows 2 mode families per a single mode spacing, whereas the scattering through the angles of 10° to 60° shows one mode family per a single mode spacing. As expected, the angles from the 70° to 140° shows half mode family in a single mode spacing, and the angles from 150° to 170° shows one mode family per a single mode spacing. The 180° scattering (backscattering) intensity shows 4 mode families in a mode spacing.

In the perpendicular polarization case, the light intensity at the 0° (forward) scattering is same with the parallel case by having 2 mode families per a mode spacing. The number of mode families for the a single mode spacing is similar to the parallel polarization case. The light intensities from 10° to 90° present half of the mode families in a mode spacing whereas the intensities from 100° to 170° present one mode family per a single mode spacing. The intensity at 180° (backward) scattering presents 4 mode families per a mode spacing.

The explanation for this behavior is attributed to the parity symmetry of the whispering gallery modes. The simulation solves for the field expansion coefficients, where even and odd polar mode numbers of the resonances decide the outcome of the simulations

[42]. Throughout the data, if the angle is suitable, even polar mode numbers contribute to the spectrum, whereas the odd numbered polar modes do not, thereby adjusting the amount of polar mode families contributing the spectrum [51].

3.2   Gaussian beam excitation simulations of silicon microspheres

The whispering gallery modes (WGMs) in microspheres can be excited with the help of Gaussian beams with evanescent field tails. Figure 3.2 shows the diagram of the optical coupling for the microspheres with the essential parameters, where ω_o is the half width of the full maxima of the Gaussian beam, b the impact parameter, a the radius and the N_{sphere} the refractive index of the microsphere. The direction of the propagation for the beam is +z direction, whereas the polarization of the beams are determined with the direction of the electric field for TE and TM polarization cases which is always in the direction +x. TE geometry has the impact parameter initially located at y= -b and x = 0 while TM geometry has the impact parameter initially located at x = -b and y = 0. For these simulations, radius of the sphere is 500 μm, refractive index of the sphere is 3.5, ω_o is 54 μm, and the impact parameter is 555 μm, accounting for 1 μm cladding.

The simulated spectra for the angles from 0° to 180° with the Gaussian beam excitation are rich with the various WGMs [48]. The angle dependent spectra is similar to the simulation results obtained by the plane wave excitation. In the TE polarized case, which is displayed in the Fig. 3.3, the intensities at the 0° and 10° present 2 mode families

35

in a single mode spacing. The intensities at the 20° and 30° show 8 mode families whereas 40° shows 4, 50° shows 6 and 60° shows 8 polar mode families in a single mode spacing. The calculated intensity at 70° shows 2 mode families, whereas the intensities at 80° and 90° show 8 mode families. The rest of the angles are similar with the previous ones, where the intensity at 100° shows 4 mode families, 110° and 120° show 6 mode families, 130° shows 8, 140° shows 2, 150° shows 10, 160° shows 8 and 170° and 180° show 10 mode families per a single mode family.

The TM polarized case for the Gaussian beam excitation is presented in the Fig. 3.4 and it is similar to the TE polarized case, but the mode families are less visible. However, it is still possible to observe the mode families displayed in the spectra with a dependence on the polar angle. The intensities at polar angles from 0° to 40° show 6 modes, 50° and 60° show 2 mode families per a single mode spacing. The intensities from 70° to 90° show 6 mode families, 110° shows 2 mode families, 120° shows 4 mode families, 130° shows 2 mode families and the rest of polar angles from the 140° to 180° show 6 mode families per a single mode spacing.

The structure of the spectra for the Gaussian beam excitation contains an even number of mode families per a single mode spacing. This again can be explained with the parit symmetry of the polar modes displayed in a single mode spacing. As the resonance condition in the sphere is obtained, the polar modes with the even polar mode orders can be

displayed in the spectra. These numerical simulations will be usefull for the analysis of the

experimental spectra with the silicon microspheres.
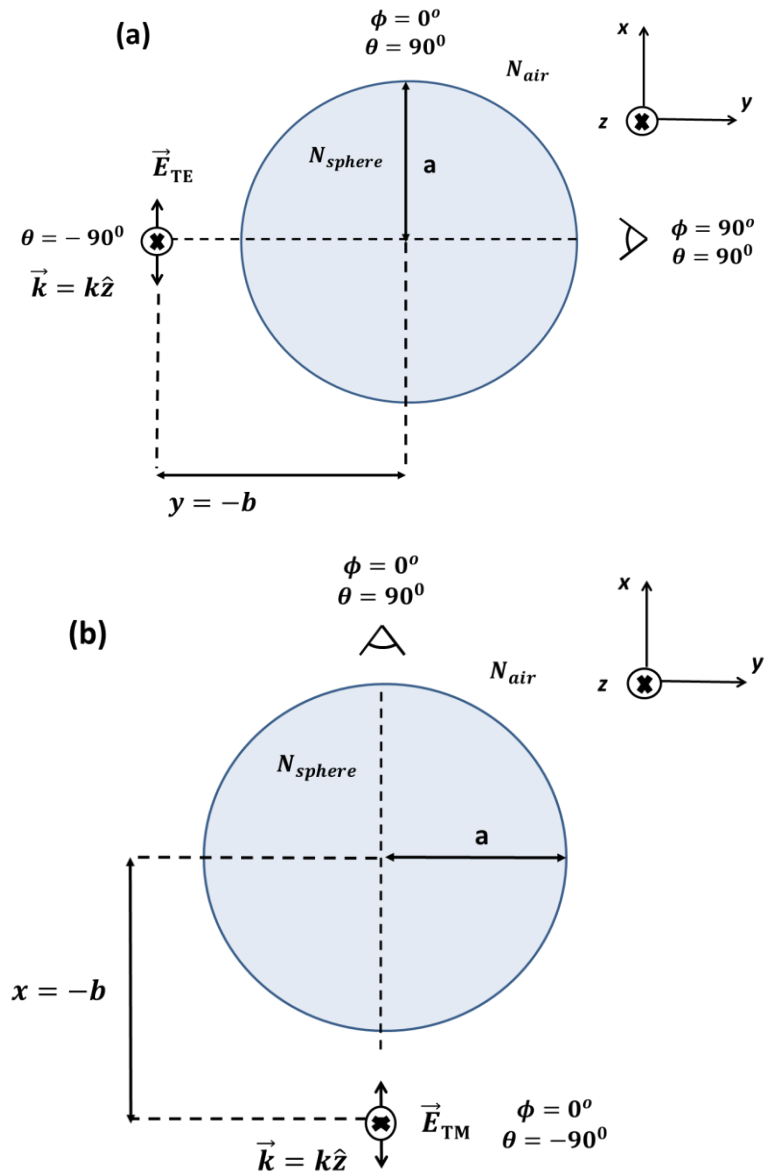
Figure 3.2: Geometry for the Gaussian beam excitation, a) TE polarization, b) TM polarization.
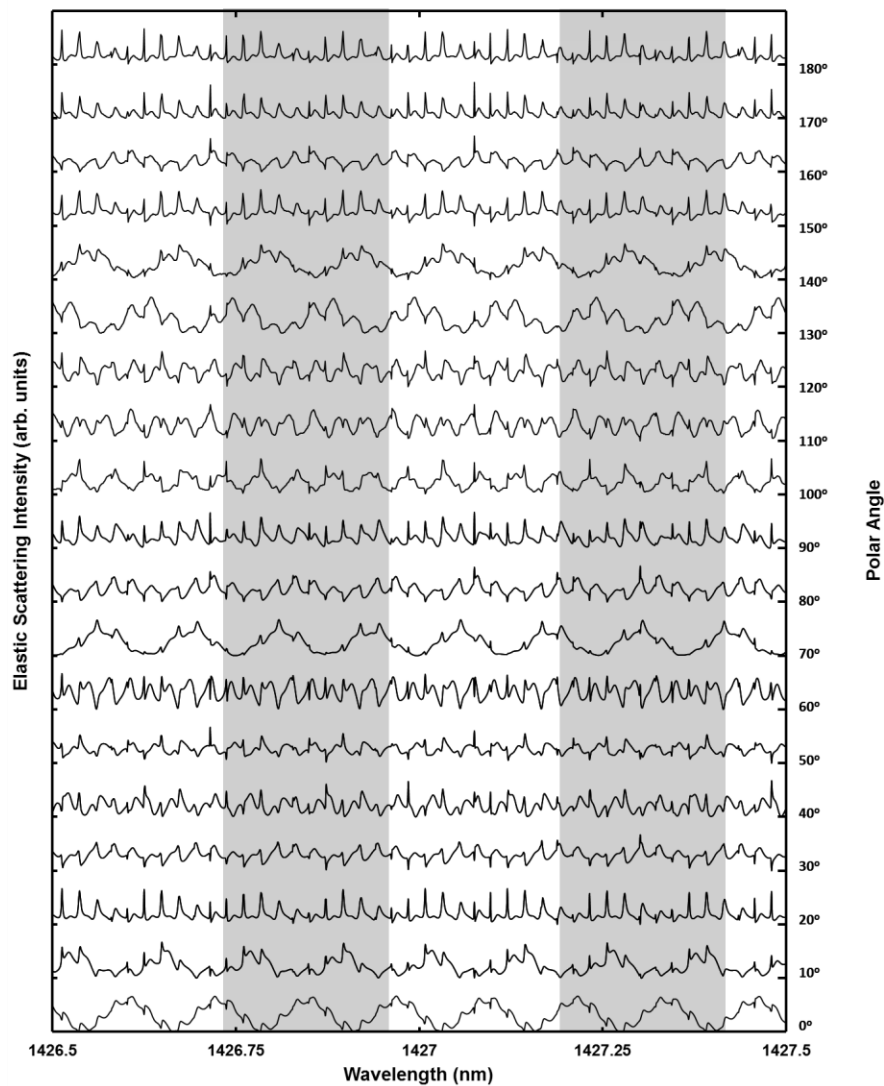
Figure 3.3: 90° Elastic light scattering with respect to the polar angle with TE polarized gaussian excitation light.
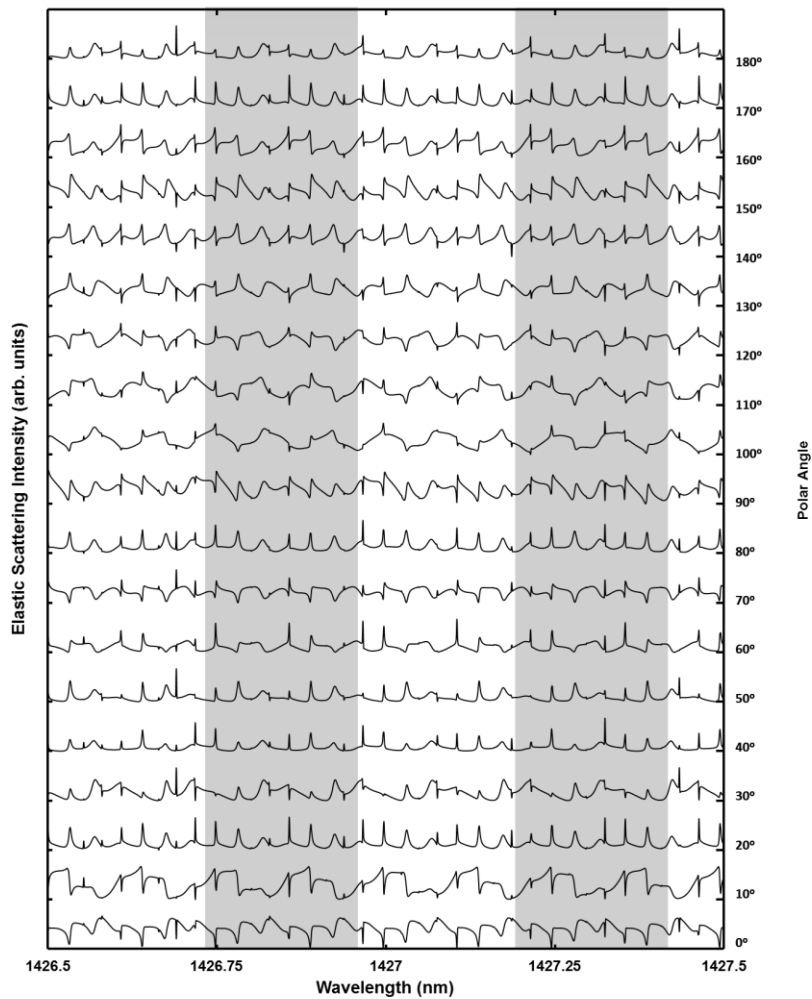
Figure 3.4: 90° Elastic light scattering with respect to the polar angle with TM polarized gaussian excitation light.

Chapter 4

Experimental Measurements on the Silicon Microsphere

This section will consist of the characterization of the physical properties of the silicon spheres and the near-infrared (near-IR) excitation laser diode together with the optical characterization setup for the elastic light scattering measurements.

4.1   Physical Properties of the silicon spheres

Physical properties of the spherical silicon microresonators will be discussed in this section. Surface and shape properties of the silicon spheres are investigated with scanning electron microscopy (SEM) and optical photography. Bulk crystalline properties were obtained with He-Ne laser excitation Raman scattering measurements, whereas the electrical characteristics are obtained with I-V measurements.

4.1.1   Surface properties of the silicon spheres

Ellipticity of the spheres was obtained by SEM photographs, which can be seen in Fig. 4.1. The spheres are found out to be slightly elliptical with ellipticity $e = 0.008$, where the long axis has a radius of $R_{long} = 504.5$ μm and the short axis has a radius of $R_{short} = 501$ μm.

Silicon spheres are commercially obtained and chosen for their low surface roughness. The spheres were cleaned thoroughly with hot ethanol and water solution bath in an ultrasound cleaner and figure 4.1 shows a relatively smooth sphere surface with miniscule defects.
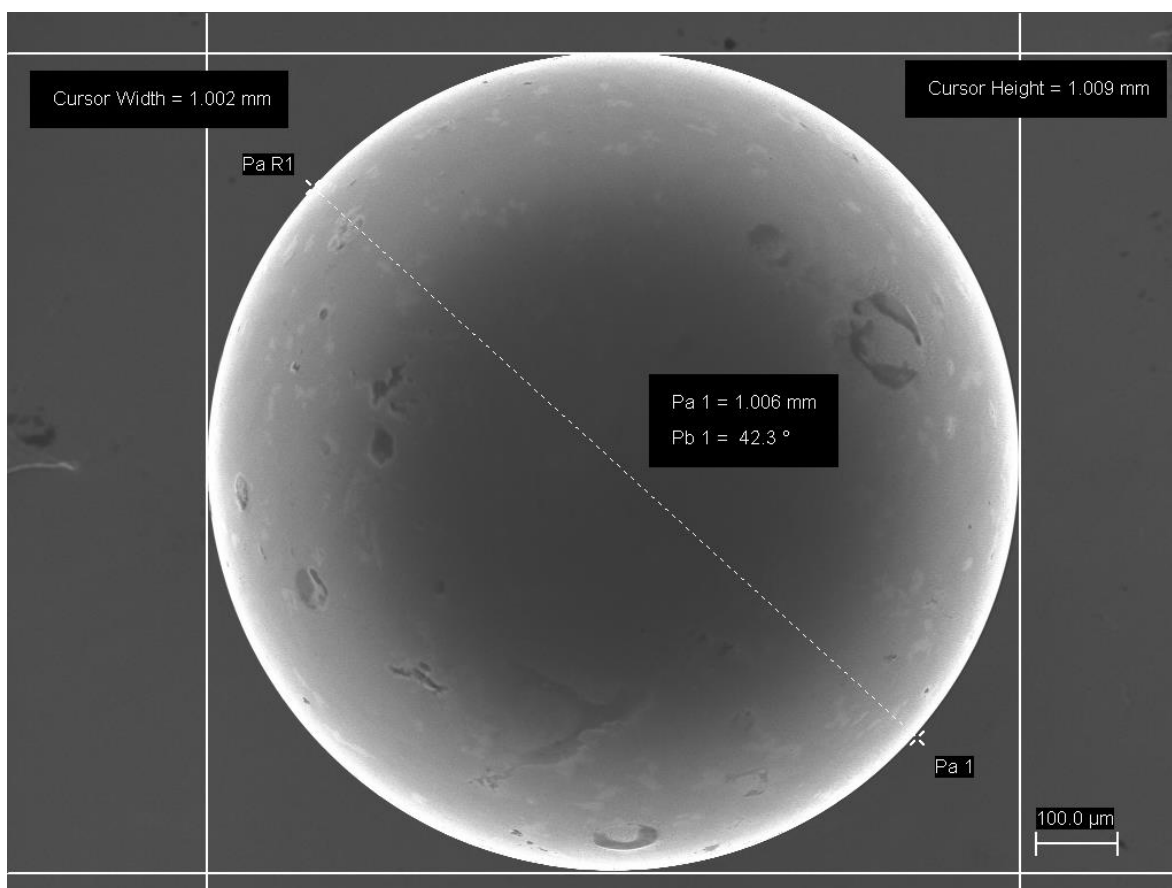
Figure 4.1: Photograph of a silicon sphere obtained by SEM measurements.

4.1.2   Raman scattering spectrum of the silicon microsphere

The structure of the silicon spheres is determined with the Raman spectroscopy. The measurements are performed in room temperature (300 K) and can be seen in Fig 4.2. The

excitation source is a He-Ne laser with a wavelength of 632.8 nm, whereas the resolution of the measurement is 0.7 cm^{-1}. The largest peak is located at the 520 cm^{-1}, which shows the first order optical phonon vibration excited by the input laser [52]. This peak has narrow linewidth and high accuracy for the vibration frequency, which indicates the purity of the crystalline structure of the silicon microsphere.
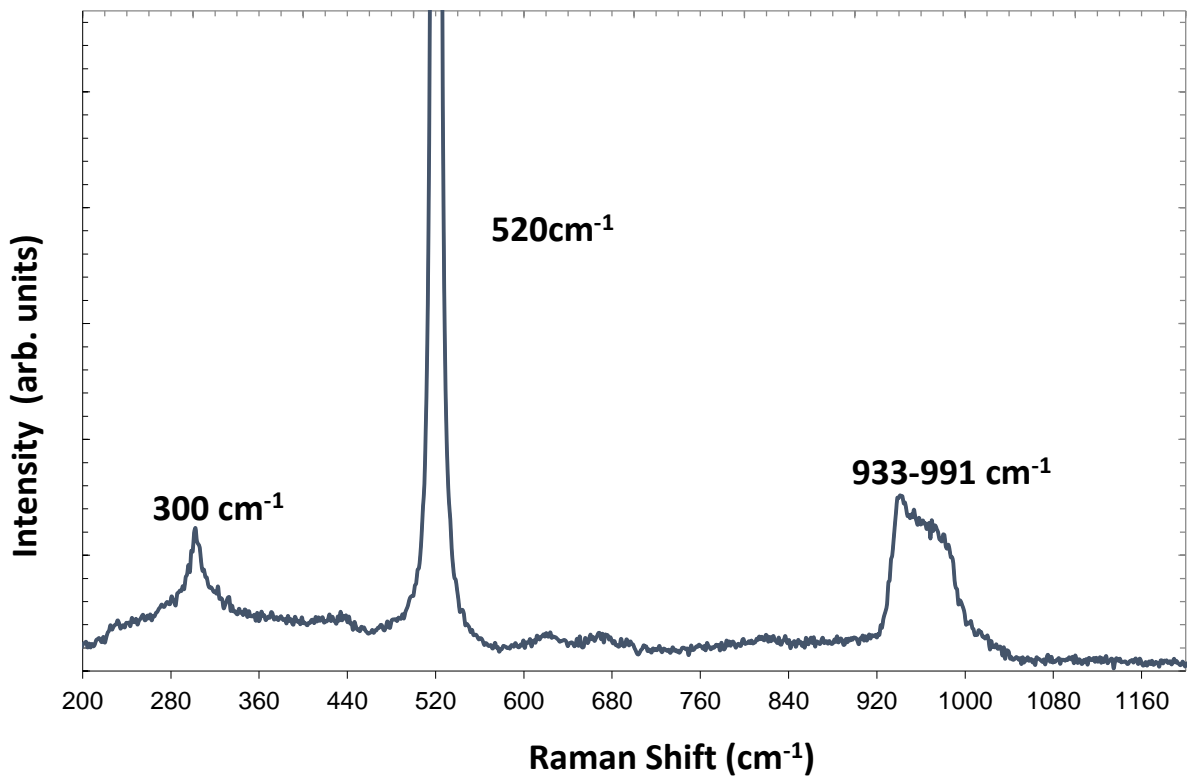
Figure 4.2: Raman spectra of a polished silicon sphere with 632.8 nm excitation.

The broadband observed for 933-991 cm^{-1} and the narrow peak located at 300 cm^{-1} indicate the second order Raman scattering from the silicon lattice [53]. The peak at 300

cm^{-1} shows the secondary transverse acoustic phonon interaction, whereas the broad band at 933-991 cm^{-1} shows the secondary transverse optical phonon interaction [54]. Minor peaks in the Stokes side of the spectrum show miniscule intensities (< % 1) and do not correspond to the known phonon interactions of the crystalline silicon, thus they can be regarded as the contamination left on the sphere by the environmental effects (such as native oxides created by air).

4.1.3   Electrical properties of the silicon spheres

The electrical characterization of the spheres can be seen in figure 4.4. The measurements were taken with metallic probe contacts holding the silicon sphere from the sides (fig. 4.3a). This arrangement is expected to have a metal-semiconductor-metal (MSM) Schottky type I-V behavior. The response of the silicon sphere is slightly asymmetric on the positive current side (fig. 4.3b) due to the non-symmetric metal probes [55].

(a)
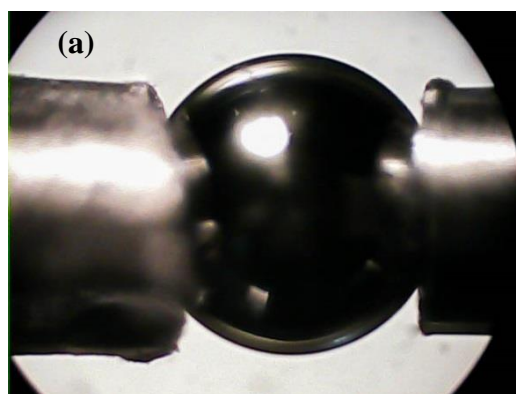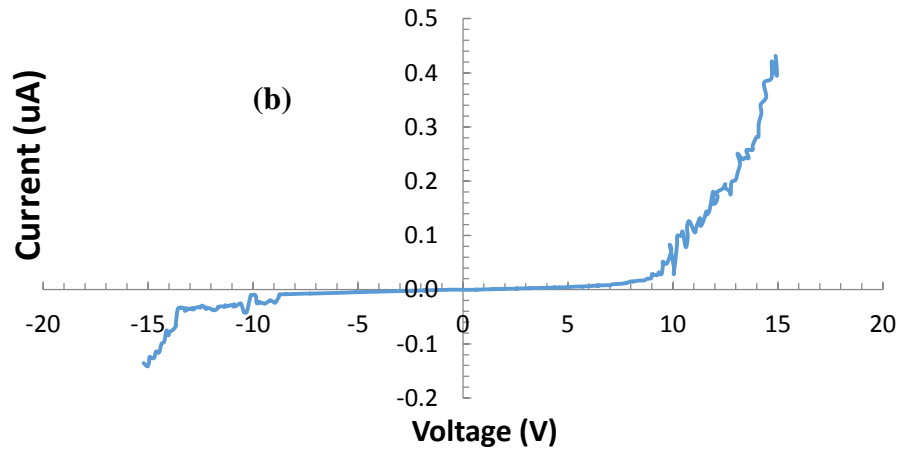
Figure 4.3: a) Optical photograph for the sphere with metallic probes, b) I-V characteristic of the metal silicon metal contacts.

4.2   Laser diode temperature-wavelength characterization

A near-IR telecommunication distributed feedback (DFB) laser diode with a temperature tunability was used in the experiments [56], [57]. The laser diode has a butterfly type package for electrical contacts and a fiber pigtail for optical output. The diode is mounted on a thermo-electric control (TEC) module, which adjusts the temperature of the cavity with a TEC current. The change in temperature adjusts the cavity length of the diode laser and determines the wavelength of the output light. The diodes can be calibrated over the wavelength with a dependence on TEC thermistor resistance (R) in ohms and the temperature (T) in kelvin given as:

$$\frac{1}{T} = C_1 + C_2 \ln(R) + C_3 \ln(R)^3 \tag{4.1.}$$

The above equation is known as Steinhart-Hart curve for thermistors. The constants C_1, C_2 and C_3 determine the resistance of the thermistor. The characterization curves for the wavelength tuning range of the laser diode can be seen in figure 4.4.
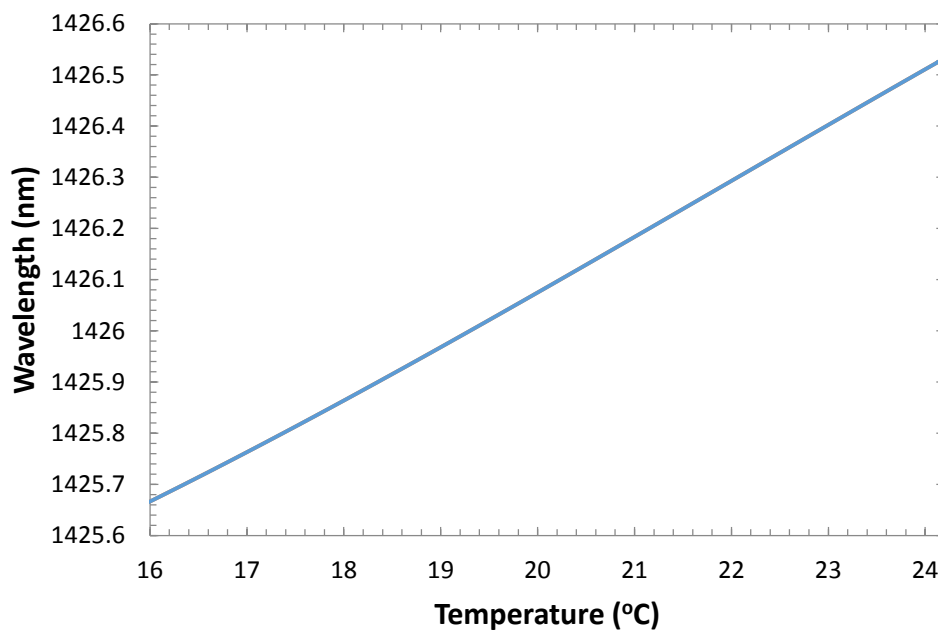
Figure 4.4: Temperature vs wavelength calibration curve for the laser diode.

4.3   Optical setup for the characterization of the resonances

In this section, the experimental setup for the creation of optical resonances will be presented. The parts of the setup consist of spherical silicon microresonator, fiber optics, photodetectors and laser diodes. All of the equipment is characterized for electrical, physical and optical properties and a setup diagram is given in figure 4.5.

A tunable laser diode with IR light output is used for the experiments in the fiber optical coupling setup, where laser light is transmitted via a single mode optical fiber. The evanescent coupling was achieved with an optical fiber half coupler (OFHC) and micro-position control of the sphere over the OFHC, while the data were obtained with detectors positioned at the 0° transmission and 90° elastic light scattering. High quality factor resonances in the elastic light scattering spectra were obtained by tuning of the input laser.
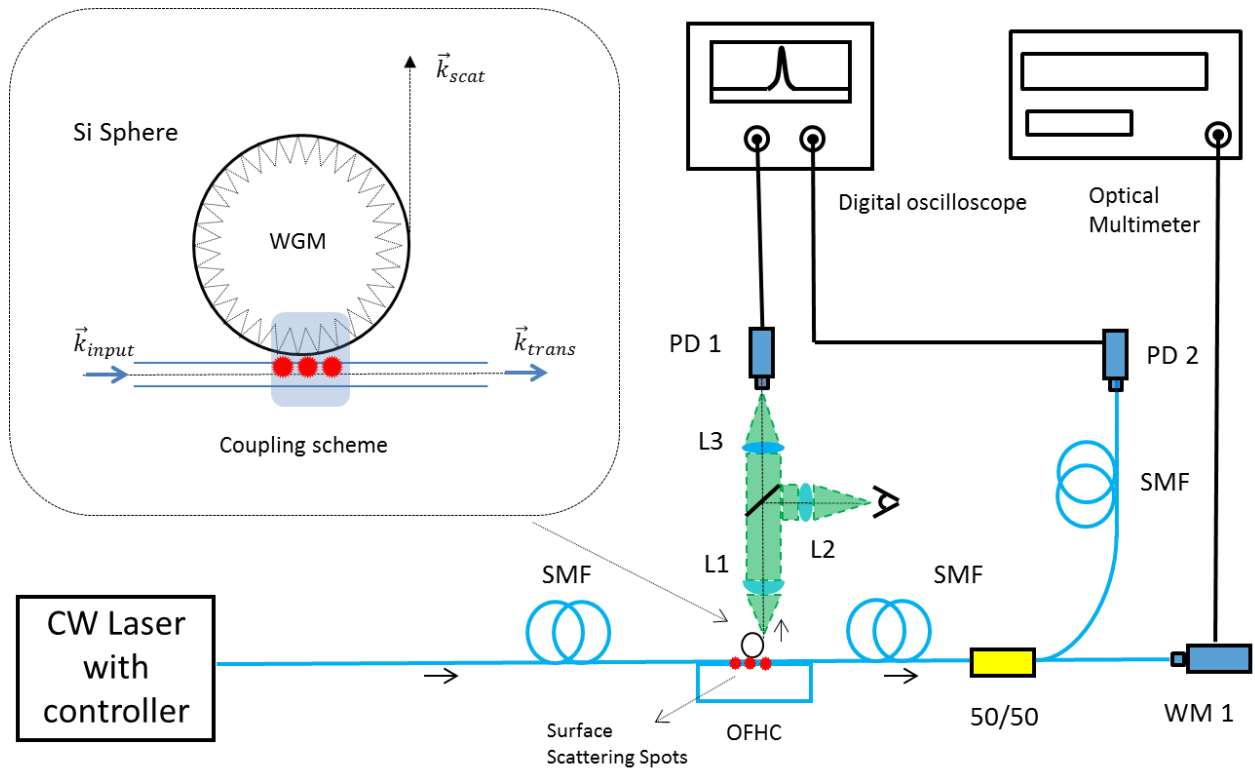
Figure 4.5: A schematic of the experimental setup. The inset shows the wave vectors of the light over the silicon sphere and the OFHC, which evanescently couples the light to the sphere with the surface scattering spots.

Figure 4.5 shows a schematic diagram of the experimental setup. The input light is supplied by a continuous wave (CW) laser operating in near-infrared (near-IR), whereas the output of the laser is butt-coupled to a single mode fiber (SMF). The input light is transmitted through the fiber and arrives at the OFHC, which couples the light to the sphere evanescently on the surface scattering spots (fig. 4.1 inset). The light scatters from the sphere in both 0° ($\vec{k}_{trans}$) and 90° ($\vec{k}_{scat}$), while a microscope lens arrangement (L1, L2 and L3) is used to collect the light in 90° and detect it with a photodetector of (P1). The 0° scattered light from the sphere is transmitted through the fiber and arrives at the 50/50 fiber coupler. This section is used for directing the light to both photodetector (P2) and a wavemeter (WM1). PD2 is used to detect the intensity variations on the 0° scattering and WM1 is used for wavelength and optical power detection. The inset in figure 4.1 shows the coupling of light into a whispering gallery modes (WGMs) of the silicon microsphere. The overall data acquisition is achieved by GPIB connection of the digital storage oscilloscope and optical multimeter to the computer.

4.4   The Coupling Scheme with the Optical Fiber Half Coupler

The optical fiber half coupler (OFHC) acts as a waveguide for the excitation light (figure 4.6). The OFHC is a glass block with a single mode fiber embedded on the top surface of the block [58]. An optical fiber is stripped from the buffer and its cladding is polished close to the core. The incoming light is coupled out of the polished fiber and

forms a region of evanescent light wave over the glass block, which couples the light to the

sphere in close proximity (figure 4.7).
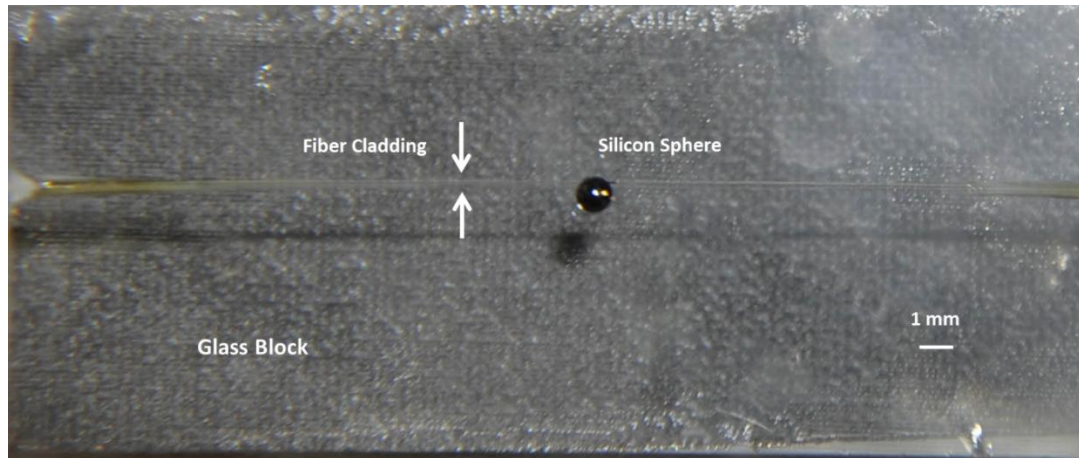
Figure 4.6: Photograph of the OFHC surface with a silicon sphere.
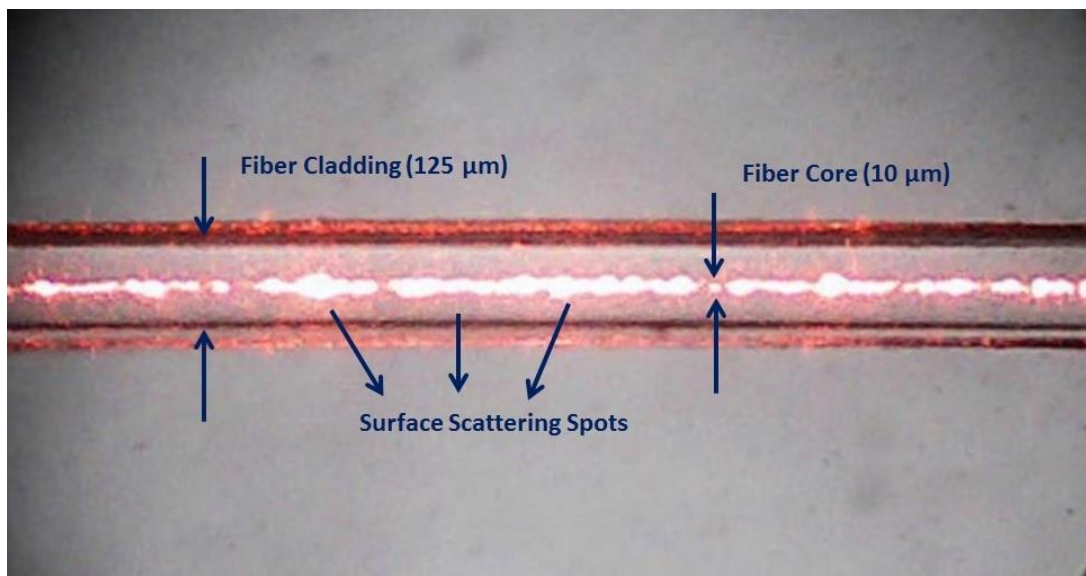
Figure 4.7: Microphotograph of OFHC with the red illumination laser.

Chapter 5

Experimental Results and Data Analysis

In this section, measurements of the optical resonances in a silicon microsphere will be presented. The experimental results can be explained by the waveguide coupled mode theory [59] with the near-IR optical resonances being excited with the Gaussian beam of a distributed feedback (DFB) diode laser, which is coupled with an optical fiber half coupler (OFHC) to the microsphere. The results are distributed into sections, where the first section shows the elastic light scattering spectra of the optical resonances. Spectral mode spacing, linewidth, and quality factor analysis are performed on these spectra. The following section presents spectrum with asymmetrical Fano like lineshape in the 90° elastic light scattering. This part is analyzed with the interference of the surface scattering with the optical resonances excited in a silicon microsphere with an OFHC. Fano like optical resonances observed in the 90° elastic light scattering are expected to be practical for filtering [60], [61], [62] and fast switching applications [63], [64]. The chapter concludes with a possible application of the silicon microspheres for biosensing [65].

5.1   The Polar Mode Spacing and the Quality Factor measurements

The determination of the mode spacing in an elastic light scattering spectrum relies on a few factors. As it is given in the chapter 2, the polar mode spacing of the resonances can be calculated by:

$$\Delta\lambda_n = \frac{\lambda_R^2 \tan^{-1}\sqrt{N_{rel}^2 - 1}}{2\pi a\sqrt{N_{rel}^2 - 1}} \tag{5.1},$$

where $N_{relative}$ the relative refractive index of the microsphere resonator and λ_R the resonant wavelength of the light, and a the radius of the microsphere. This formula leads to a theoretical mode spacing, which should be close to the observed mode spacing in the spectrum given in fig. 5.2. Relatedly, the quality factor of the resonances can be given as:

$$Q = \frac{\lambda_R}{\delta\lambda} \tag{5.2},$$

where $\delta\lambda$ is the linewidth of the resonances observed at the wavelength λ_R.

Figure 5.1 shows the elastic light scattering spectra for a silicon sphere excited by near infrared light in air. The upper curve (red) shows the transmission intensity whereas the lower curve (green) shows the 90° elastic light scattering intensity. The input laser is tuned over a temperature range from 24.3^{o}C to 18°C, which corresponds to a wavelength scan from 1425.86 nm to 1426.51 nm.

As estimated in the elastic scattering Gaussian beam calculations in the chapter 3, there are 4 mode families in a mode spacing and families appear to be smoothed. This behavior can be attributed to the wavelength resolution of the scan, where the temperature resolution is defined by the thermoelectric current (TEC) step values. This measurement is carried out with TEC steps of 1 mA, for a TEC limit of 250 mA. The change of the diode current, adjusts the resistance of the diode, thus changes the temperature of the laser diode. As described in section 4.2, the temperature change of the laser diode has a linear relation with the wavelength of the output of the laser. For a temperature range of 6.3°C and a wavelength range of 0.65 nm, the wavelength resolution of the scan presented in Fig. 5.1 results to be 2.6 pm.

Although the optical resonances appear to be smoothed, the spectrum allows the determination of the mode spacing. Since the resonant mode families show the corresponding dip and peak structure with visible polar mode families, the polar mode spacing is shown in the figure, with an average measured mode spacing of $\Delta\lambda_n = 0.24$ nm. The quality factor (Q) of the peaks in the spectrum of Fig 5.1 are on the order of 10^4.

Figure 5.1: 0° and 90° elastic light scattering spectra by a silicon microsphere in air.

Figure 5.2 shows elastic light scattering spectra for a silicon sphere excited by near infrared light in air. The upper curve (red) shows the transmission intensity, whereas the lower curve (green) shows the 90° elastic light scattering intensity. The input laser is tuned over temperature from 24.3^oC to 18.5^oC, which corresponds to a wavelength scan from 1425.91 nm to 1426.51 nm. This measurement is carried out with TEC steps of 0.5 mA for a TEC limit of 250 mA, which yields to 500 current steps. For a temperature range of 5.8^oC

52

and a wavelength range of 0.6 nm, the wavelength resolution of the scan presented in Fig. 5.2 is 1.2 pm.

As can be seen from fig. 5.2, the mode spacing of this measurement is found out to be $\Delta\lambda_n$ = 0.238 nm with a slight difference from the calculated mode spacing of 0.23 nm. As estimated, there are 4 mode families in a mode spacing. This measurement is similar to the measurement of fig. 5.1, while having a higher resolution and might be showing some of the azimuthal modes situated on top of the mode families.
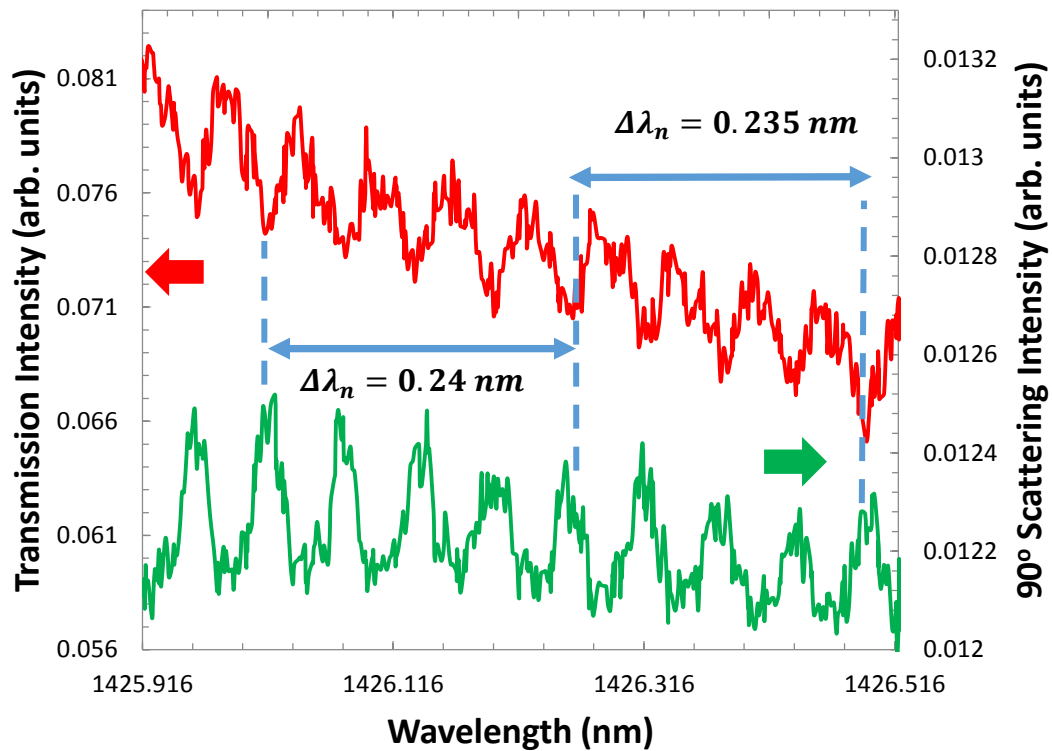
Figure 5.2: Higher resolution 0° and 90° elastic light scattering spectra by a silicon microsphere in air.

The modes of the spectrum displayed in Fig 5.2 contains high Q resonances. The transmission spectrum appears to show finer optical resonances, where the resonance located at 1426.095 nm has a linewidth of 5.3 pm, which corresponds to a quality factor of $Q = 2.7 \times 10^5$.
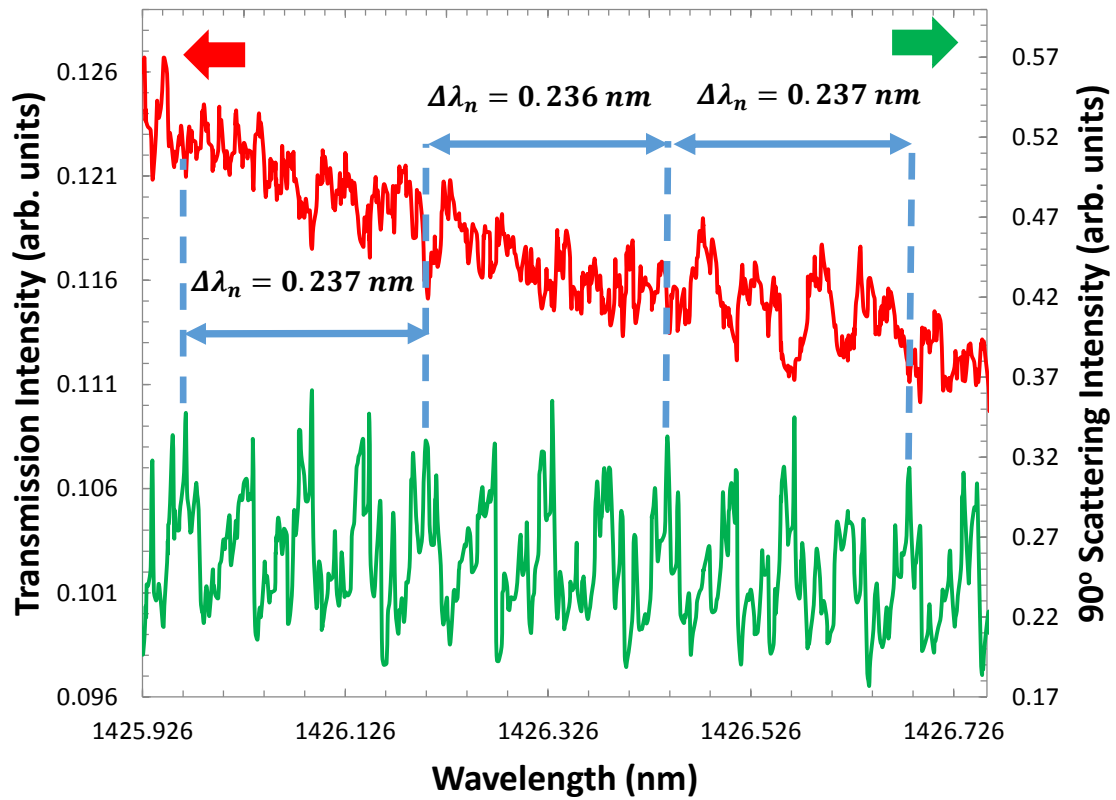
Figure 5.3: High resolution 0° (transmission) and 90° elastic light scattering spectra from a silicon microsphere in air.

Figure 5.3 shows elastic light scattering spectra for a silicon sphere excited by near infrared laser in air. The upper curve (red) shows the transmission intensity, whereas the

lower curve (green) shows the 90° elastic light scattering intensity. The input laser is tuned over temperature from 26.7^oC to 18.6^oC with a tuning range of 8.1^oC, which corresponds to a wavelength scan from 1425.92 nm to 1426.75 nm with a wavelength tuning range of 0.83 nm. There are 4 mode families in a single polar mode spacing as expected and mode clusters in the polar mode envelope are visible.

The measurement in Fig. 5.3 is carried out with TEC steps of 0.5 mA for a TEC limit of 500 mA. For a temperature range of 8.1^oC and a wavelength range of 0.83 nm, the wavelength resolution of the scan presented in fig. 5.3 results to be 0.8 pm. The 90° elastic light scattering of the figure 5.3 presents finer optical resonances. These resonances are located as clusters in the mode family envelopes. The light scattering in this measurement also shows large quality factors; mode clusters on the polar mode envelopes are more visible. As can be seen from fig. 5.3, the mode spacing of this measurement is found out to be $\Delta\lambda_n = 0.236$ nm with 4 mode families in a mode spacing. The quality factor (Q) of the peaks of the spectrum in fig 5.3 contains many high quality factor resonances. The 90° elastic scattering spectrum appears to contain finer optical resonances, where the resonance located at 1426.207 nm has a linewidth of 7.1 pm, which corresponds to a quality factor of $Q = 2 \times 10^5$.
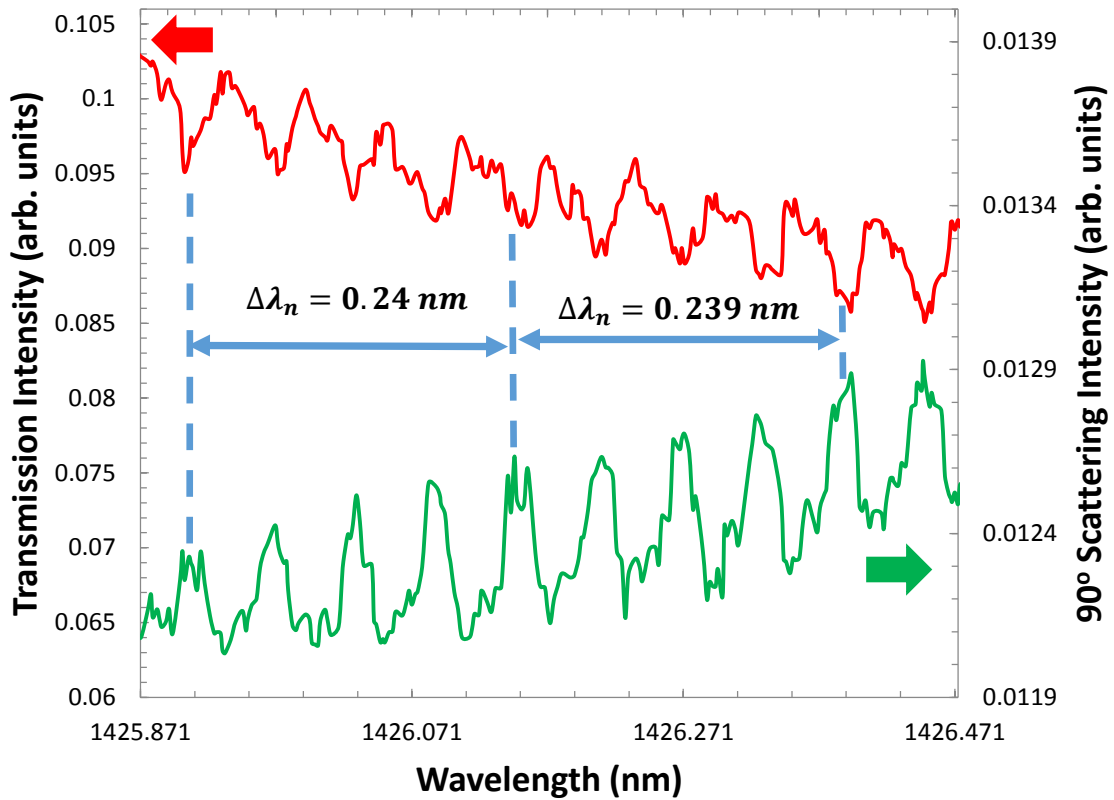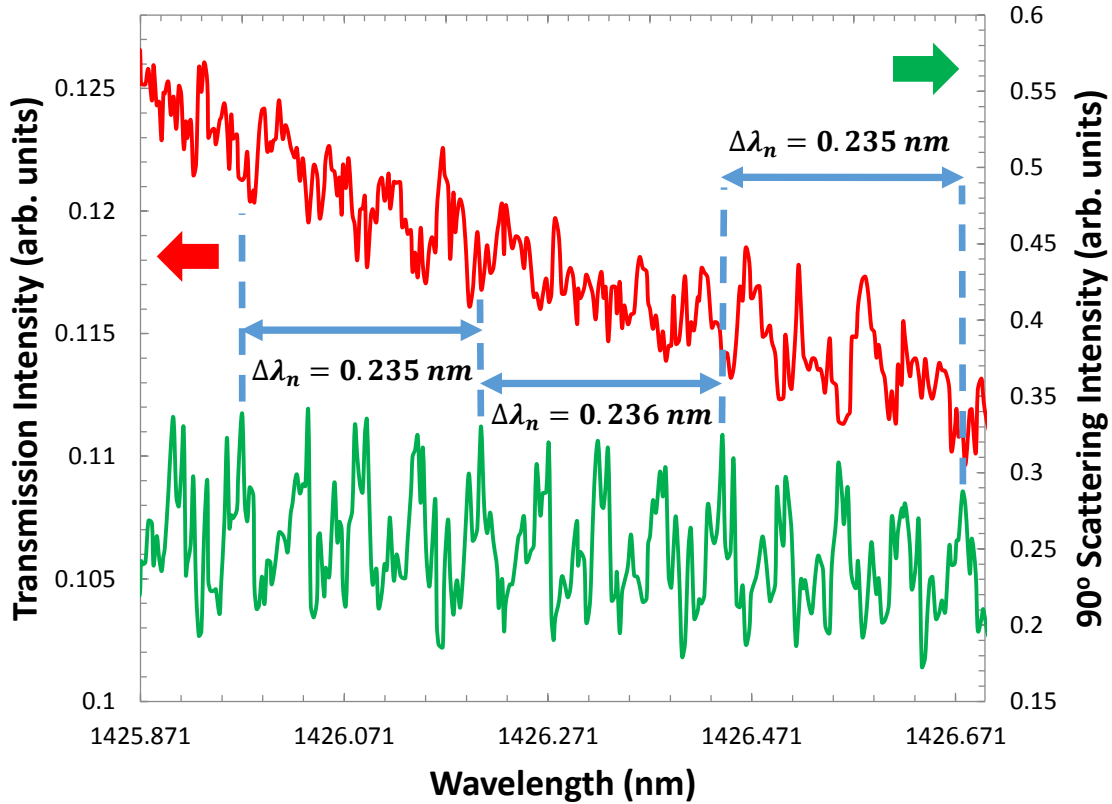
Figure 5.4: 0° and 90° elastic light scattering spectra by a silicon microsphere in air.

Figure 5.4 shows elastic light scattering spectra for a silicon sphere excited by near infrared laser in air. The upper curve (red) shows the transmission intensity, whereas the lower curve (green) shows the 90° elastic light scattering intensity. The input laser is tuned over temperature from 26.3^oC to 18.25^oC with a tuning range of 8^oC, which corresponds to a wavelength scan from 1425.87 nm to 1426.7 nm with a tuning range of 0.83 nm. There are 4 mode families in a single mode spacing and a cluster of modes are clearly visible in the spectrum.

The measurement in fig. 5.4 is carried out with TEC steps of 0.1 mA for a TEC limit of 250 mA. For a temperature range of 5.8°C and a wavelength range of 0.83 nm, the wavelength resolution of the scan presented in fig. 5.4 is 0.1 pm. The 90° elastic light scattering of the figure 5.4 presents finer optical resonances. These clusters of resonances are located in the mode family envelopes. The light scattering in this measurement also shows high quality factors; clusters of optical resonances are more visible.

As can be seen from fig. 5.4, the mode spacing of this measurement is found out to be $\Delta\lambda_n$ = 0.235 nm with 4 mode families in a mode spacing. The quality factor (Q) of the peaks of the spectrum in fig 5.4 contains high Q resonances. The transmission spectrum appears to show finer optical resonances, where the resonance located at 1426.205 nm has a linewidth of 5.3 pm, which corresponds to a quality factor of $Q = 5.5 \times 10^5$.

	Figure 5.1	Figure 5.2	Figure 5.3	Figure 5.4
$\delta\lambda$resolution	2.6 pm	1.2 pm	0.8 pm	0.1 pm
$\Delta\lambda_n$	0.24 nm	0.238 nm	0.236 nm	0.235 nm
$\Delta\lambda_c$	-	-	8.8 pm	8.8 pm
Q	~10^4	2.7×10^5	2.0×10^5	5.5×10^5

Table 5.1: Observed optical resonance parameters in the 90° elastic light scattering intensity of the measurements 1-4.

5.2   Clustering of the modes in the spectra

The 90° elastic light scattering intensity measurements of the figures 5.3 and 5.4 show a matching behavior, which can be seen in Figure 5.5. Mode families are distributed with a mode spacing of $\Delta\lambda_n$ = 0.236 nm for both of the measurements. Observed WGMs might have a mode splitting.
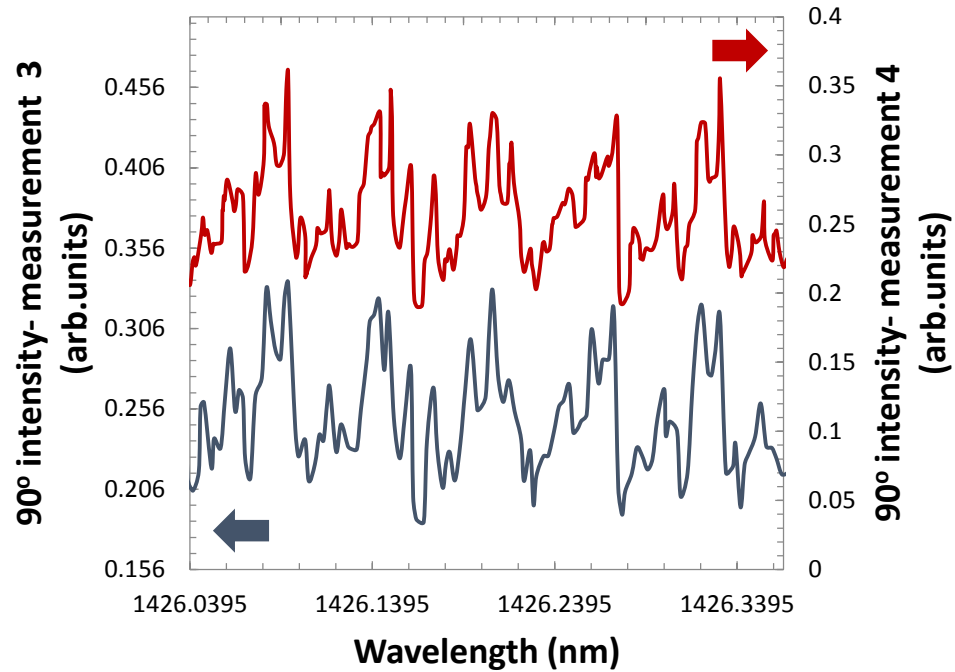
Figure 5.3: 90° elastic light scattering intensities for measurements 3 and 4.

The azimuthal mode splitting of the optical resonances in a microsphere arise from the ellipticity of the resonator [66]. Ideally, the resonator is a perfect sphere; in this case

azimuthal resonances are degenerate with *2n+1*. If the ellipticity of the microsphere is included, the position of the resonances on the wavelength can be given as [67]:

$$\lambda(m) = \lambda_R \left\{ 1 + \frac{e}{6} \left[1 - \frac{3m^2}{n(n+1)} \right] \right\}$$ (5.3),

where *e* is the ellipticity of the resonator, λ_R is the resonant wavelength, *n* is the polar mode number and *m* is the azimuthal mode number. Since the azimuthal resonances can have values between *–n* to *+n*, the wavelength of the azimuthal resonances would have a corresponding range.

One can define a mode spacing for the azimuthal modes by differentiating between the wavelengths of the consecutive azimuthal modes of order *m* and *m+1* as:

$$\Delta \lambda^m = \frac{e \lambda_R}{2} \left| \frac{2m+1}{n(n+1)} \right|$$ (5.4).

The azimuthal mode number depends on the polar mode number by having values between *–n* to *+n*. For a silicon microsphere of ellipticity *e* = 0.007 and a resonant wavelength of 1426.216 nm, the mode number *n* would be 7710. In order to have high angular momentum azimuthal modes, $n \approx m$, the azimuthal mode spacing would be 1.48 pm. This is close to the observed mode cluster wavelength difference of 8.8 pm in the 90° elastic scattering of figure 5.5.

In order to explain the excess wavelength difference in the mode cluster observed in the spectra, a few possibilities can be considered. The particle binding induced mode splitting [68], [28], [69] can be another likely candidate for the observed discrepancy. Ideally,

WGMs in a microsphere resonator has a clockwise (CW) and counterclockwise (CCW) modes with degenerate wavelengths. However, when a small particle binds on the surface, the particle causes a scattering from one of the resonator modes (CW) into the free space, whereas the CCW mode would be scattered back in the opposite direction. This would create a mode splitting depending on the quality factor of the resonator [70].

In more theoretical terms, the mode splitting can be explained by the coupling strength (g) of the modes and the linewidth broadening ($\varGamma_R$) induced by the splitting [9], [71]. The coupling strength is determined by the the azimuthal splitting with $g = \pi\varDelta\lambda_c$, where $\varDelta\lambda_c$ is the observed wavelength detuning of the mode cluster. The linewidth broadening is $\varGamma_R = \pi|\delta\lambda_1 - \delta\lambda_2|$, where $\delta\lambda_1$ and $\delta\lambda_2$ are the linewidths of the split modes. When the particle is much smaller than the excitation wavelength ($R_{particle} << \lambda_R$); the particle interaction with the evanescent field of the WGM induces a dipole moment depending on the particle polarizability (α) as:

$$\alpha = 4\pi R_{particle}^3 \frac{(\varepsilon_p - \varepsilon_m)}{(\varepsilon_p + 2\varepsilon_m)} \qquad (5.5),$$

where the ε_p and ε_m are the electric permitivities of the particle and the medium. The above formula requires the refractive index of the particle to be known, since it depends on the electric permittivity. However, the polarizability of the particle might be found depending on the g and $\varGamma_R$. The parameters are given as:

$$g = -\alpha^2 f^2(r) \frac{\pi c}{\lambda V_{WGM}} \qquad (5.6),$$

where *f(r)* is the normalized mode distribution and V_{WGM} is the mode volume. Relatedly, the linewidth broadening of the resonances can be found as:

$$\Gamma_R = \frac{4c\pi^3\alpha^2 f^2(r)}{3\lambda_R V_{WGM}} \tag{5.7}.$$

Combining the equations 5.5 and 5.6; one can find the polarizability of the particle by only measuring the linewidth broadening and the mode shift of the spectrum, as:

$$\alpha = \left(\frac{-3\lambda^3}{8\pi^2}\right)\left(\frac{\Gamma_R}{g}\right) \tag{5.8}.$$

The particle radius is related with the dielectric permittivity described with the equation 5.5, by combining the equation 5.5 with the equation 5.8, the radius of the particle depending on the ratio (Γ_R/g) and dielectric permittivity (ε_{rel}) can be written as:

$$R_{particle} = \frac{\lambda_R}{\pi}\left(\frac{3\Gamma_R/g}{32\varepsilon_{rel}}\right)^{1/3} \tag{5.9}.$$

When the clustering peaks of the figure 5.5 located around λ_R = 1426.207 nm are considered, the ratio of the cluster spacing to the mode linewidth is; Γ_R/g = 0.375. For a water droplet with a relative dielectric permittivity of ε_{rel} = 0.1471, the equation 5.9 yields to a particle radius of $R_{particle}$ = 281.74 nm, which is plausible for an accumulation of humidity layer on the sphere.

5.3   Asymmetrical lineshape in elastic light scattering

Asymmetrical lineshapes can be observed in the optical resonances [72], [73], [74], [75] and may have various applications especially in filtering [60], [61], [62] and switching [63], [64]. The Figure 5.6 shows the excitation of WGM resonances in a silicon microsphere in air. The input laser is tuned over temperature from 24.4^{o}C to 17.8 ^{o}C, which corresponds to a wavelength scan from 1426.25 nm to 1425.88 nm. The 90° elastic light scattering spectra shows asymmetrical line shapes, while the 0° transmission spectra contains Lorentzian line shapes for the WGMs. The asymmetrical lineshape observed in the 90° spectra are called Fano lineshape, which may occur due to the interference between the elastic light scattering from the microsphere and the surface of the OFHC.

When the silicon microsphere is coupled with the optical waveguide, phase sensitive interference of light can be observed. This interference occurs between the electric fields of the WGMs and the background (BG) light, which consists of the surface scattering on the OFHC and the geometric resonances (glare spot) on the microsphere [39]. WGMs contain narrow linewidth resonances, and the surface scattering of the light and geometric effects creates a DC background (BG) component in the spectrum. However, wavevectors of the WGM and the BG have a mismatch, which creates a phase mismatch between the light scattering from the BG and the light coming from the WGMs of the sphere. As a result, asymmetric lineshapes can be observed in the 90° elastic light scattering spectrum [76].
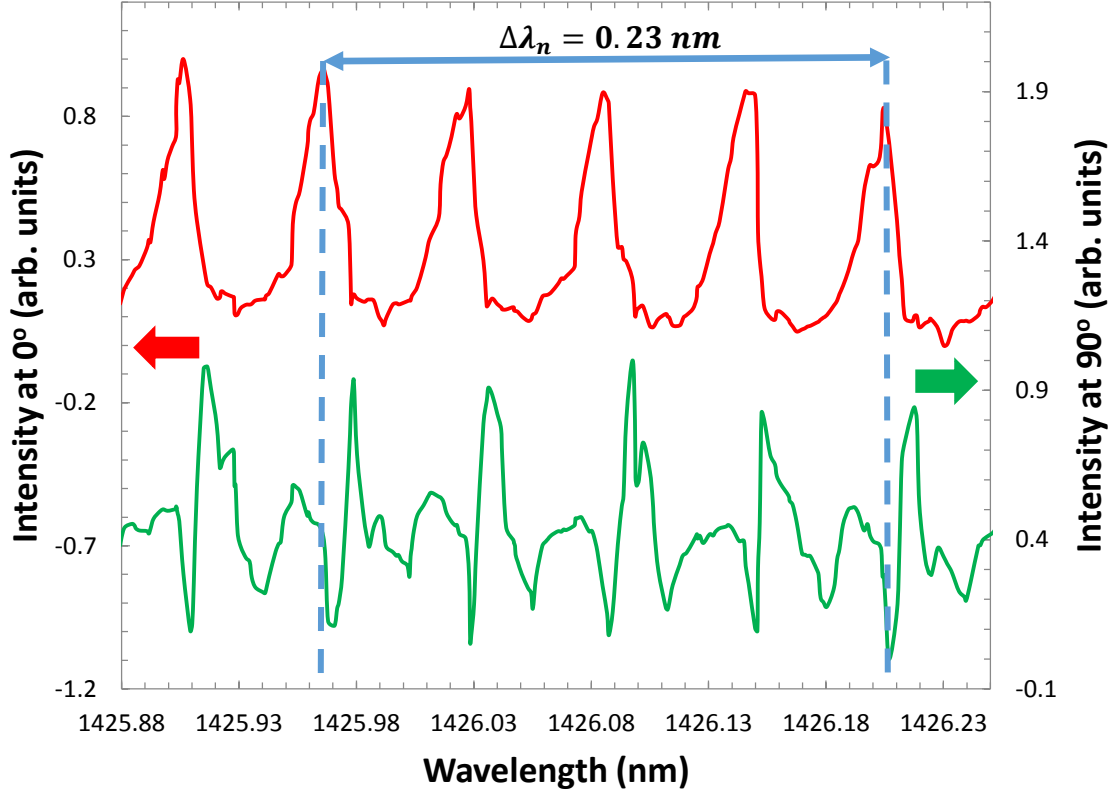
Figure 5.4: 0° transmission and 90° elastic scattering spectra from a silicon microsphere.

The total intensity obtained by a detector positioned on 90° would be dependent on the electrical fields of the WGMs and the BG as:

$$I_{total} = \frac{c\varepsilon_0}{2}\left[|E_{WGM}|^2 + |E_{BG}|^2 + 2E_{WGM}E_{BG}^* e^{i\Delta\phi}\right] \qquad (5.11),$$

$$I_{total} = I_{WGM} + I_{BG} + c\varepsilon_0 E_{WGM}E_{BG}^* e^{i\Delta\phi} \qquad (5.12),$$

where ε_o is the vacuum permittivity, E_{WGM} the electric field of the WGM, E_{BG} the background electrical field, I_{WGM} and I_{BG} the WGM and background intensities, $\Delta\phi$ the phase difference between the WGM and the background.

FABRY-PEROT (FP) ETALON OF THICKNESS 'd'   SPHERE WITH RADIUS 'a'

Input → m

0° Transmission

180° Reflection ← d

90° Scattering

m

a

Input   Transmission

INTENSITY VS WAVELENGTH

$\Delta\lambda$

FP - (180° Reflection) / Sphere - (Transmission)

FP - (0° Transmission) / Sphere - (90° Scattering)

λ_{n+3} λ_{n+2} λ_{n+1} λ_n
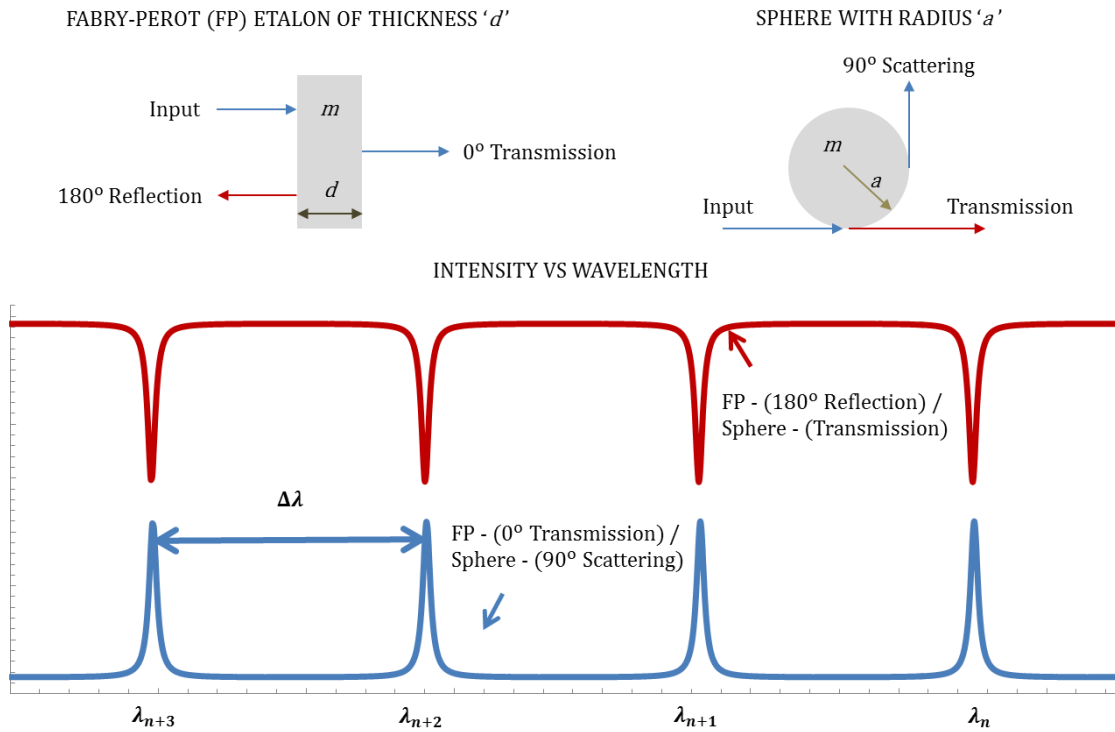
Figure 5.5. Schematic of the analogy between a Fabry-Perot etalon and a microsphere spectrum.

If an analogy to the Fabry-Perot resonator is given, the effect of the phase difference ($\Delta\phi$) between the fields can be seen clearly. In case of no absorption, the electric

field magnitude of the WGM can be expressed in terms of the transmittance (T) and reflectance (R) coefficients;

$$\frac{E_{WGM}}{E_0} = e^{i\omega t}\left[\frac{T}{1-Re^{i\delta}}\right]$$ (5.4),

where $E_0e^{i\omega t}$ is the input supplied to the microresonator and $\delta=2\pi x N_{sph}$ is the phase acquired by the WGMs. If the background fields are added, the total intensity (I_{total}) observed at 90° can be written as:

$$\frac{I_{total}}{I_0} = \left[\left(\frac{T}{1-Re^{i\delta}}\right)^2 + 2\left(\frac{T}{1-Re^{i\delta}}\right)e^{i\Delta\phi} + 1\right]$$ (5.5).

The above equation shows the dependence of the total intensity observed at 90° on the phase difference of the fields. For the specific cases of $\Delta\phi$ = 0, $\pi/2$, π and $3\pi/2$, total intensity should show symmetrical (Lorentzian) and asymmetrical (Fano) lineshapes in the spectrum. The results of this simulation can be seen through figures 5.8 to 5.11. Depending on the figures, we can conclude that the phase difference in our observed spectrum is around $3\pi/2$.
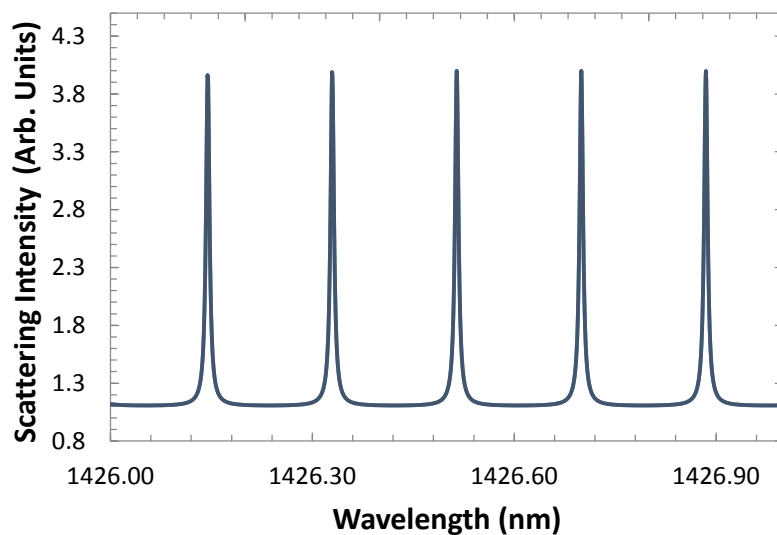
Figure 5.6: 90° elastic scattering intensity with $\Delta\phi = 0$ phase difference.
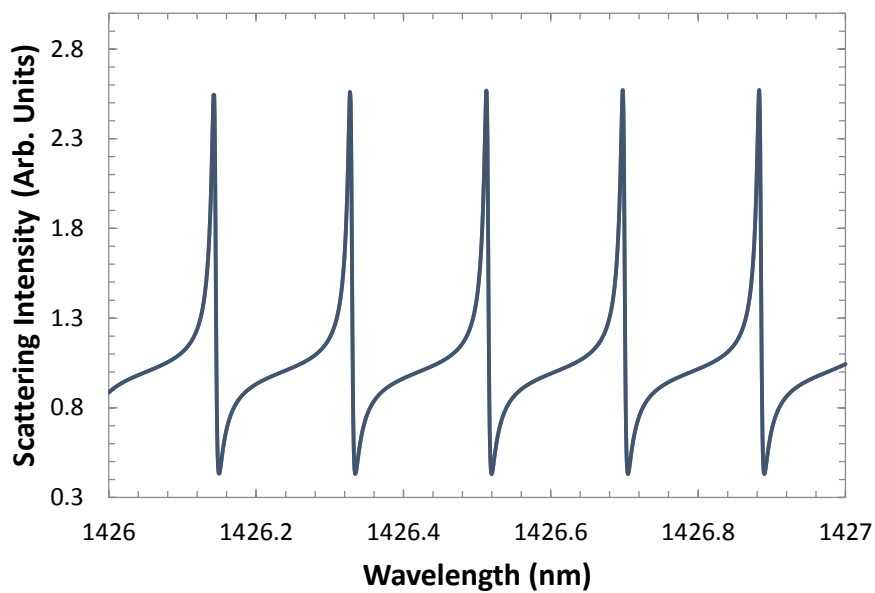
Figure 5.7: 90° elastic scattering intensity with $\Delta\phi = \pi/2$ phase difference.
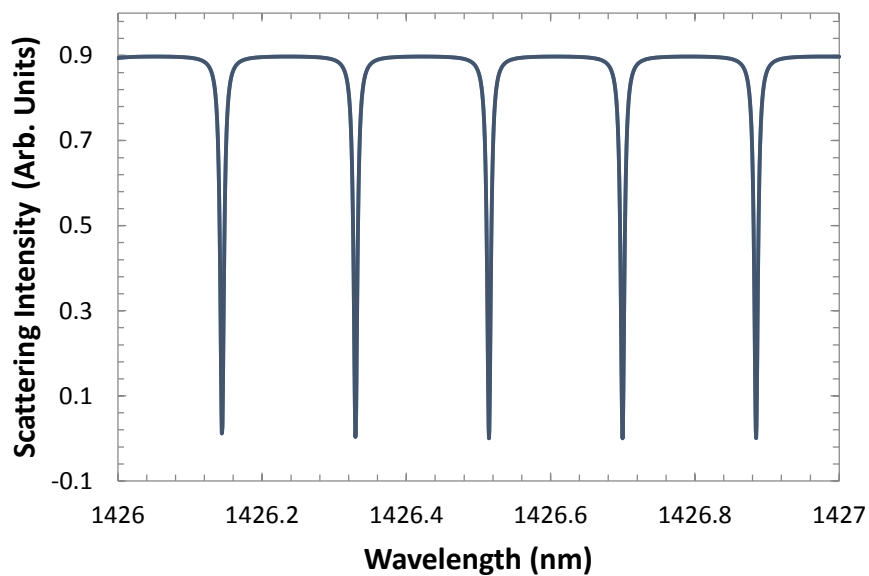
Figure 5.8: 90° elastic scattering intensity with $\Delta\phi = \pi$ phase difference.
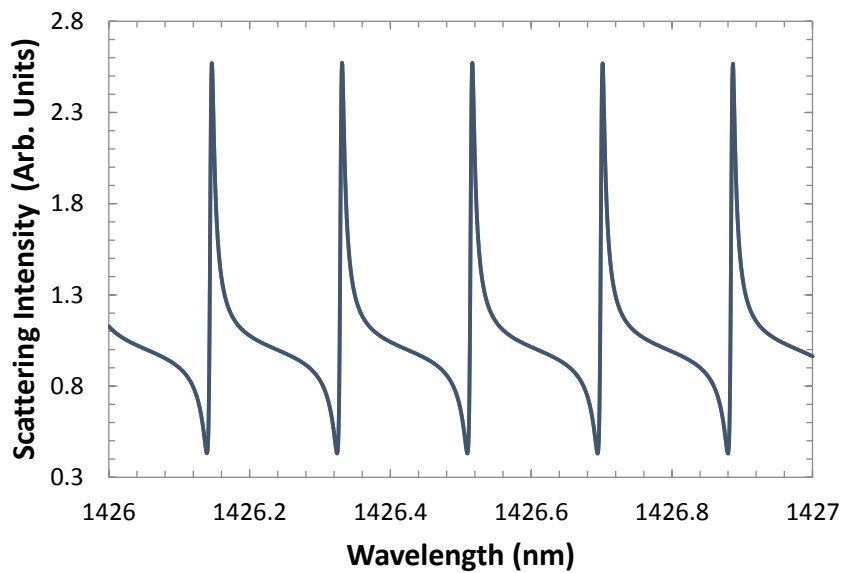
Figure 5.9: 90° elastic scattering intensity with $\Delta\phi = 3\pi/2$ phase difference.

5.4   Biosensing application with silicon microspheres

Optical resonances have found many applications for the biology and biosensing [18], [77]. Detection of the small agents such as proteins, viruses and genes can be carried out with the help of the near infrared optical resonances [7]. One way to establish this approach is to create WGMs on a microsphere and measure the small shifts on the resonant wavelength spectra. If there are small biological agents present in the environment, than the interaction of the agents with the microsphere should yield to observable changes in the spectrum.

Whenever a small particle is adsorbed on to the sphere, light modes resonating in the sphere should have slightly longer optical paths thus effectively shifting the resonant wavelength. Also, the refractive index of the material surrounding the microsphere should also contribute to the wavelength shift. Depending on the radius increase (δa) of the resonator and the refractive index change (δN) of the surrounding medium, the wavelength shift ($\delta\lambda_{shift}$) in the spectrum can be estimated as:

$$\frac{\delta\lambda_{shift}}{\lambda} = \frac{\delta a}{a} + \frac{\delta N}{N_{relative}}$$

(5.10),

where a is the radius and $N_{relative}$ is the relative refractive index of the resonator. The shift in the wavelength of the optical resonances can be detected if the linewidth of the resonances are smaller than the shift. This condition can be satisfied with the WGM resonances on dielectric microspheres excited with a narrow linewidth telecom laser.

Optical detection of the DNA with the help of the WGMs on a sapphire [78] or silicon microspheres have been proposed recently. Techniques rely on the radius increase of the microsphere together with the refractive index change of the environment due to the adsorption of the DNA base pairs in liquid buffer solutions.

When a silicon microsphere with a radius of 500 μm is immersed in the liquid mixture, a DNA layer can get adsorbed on the surface of the resonator. A base pair has a length of approximately 0.33 nm, thus, a DNA layer of 10 nm can accumulate on the surface with 30 DNA base pairs. This should bring a wavelength shift of 0.03 nm with a standard telecom laser operating at 1426 nm. On the other hand, refractive index change in the mixture created by the adsorbed DNA material would also contribute to the wavelength shift. If the DNA molecules crate a refractive index change of $\delta N = 0.001$ in a phosphate buffer saline (PBS) solution with a refractive index of $N_{PBS} = 1.335$, than the wavelength shift of the optical resonances due to the index change of the mixture would be 0.54 nm with an operating wavelength of $\lambda = 1426$ nm. Overall, the expected resonant wavelength shift would be 0.57 nm, which is much larger than the linewidth (1.2 pm) of the observed light resonances on the silicon microspheres. The mode spacing of the silicon microspheres is 0.23 nm, which is also smaller than the wavelength shift, thus the presence of the DNA molecules can be detected by the WGMs of a silicon microsphere with a moderate accuracy.

Chapter 6

Conclusions

A summary of the work together with the conclusions obtained from the thesis will be given in this chapter. The thesis starts with the review of the microsphere optical resonators, where the characteristics of the spherical WGM resonators are discussed. After this part, the coupling of light to the microspheres is described. Optical coupling to the microspheres is affected by the shape of the excitation beam and with the nature of coupling. Coupling mechanisms are listed as optical fiber half coupler (OFHC), prism, fiber tip and tapered fiber, where OFHC method is used in the experimental part of this thesis. Overall, the first chapter describes the applications of the microsphere resonators together with the efficient mechanism for the optical coupling.

Chapter 2 gives the theoretical background for the optical resonances in spherical particles. The chapter starts with geometrical description of the total internal reflection (TIR) where, this phenomenon gives rise to the trapping of the light in a symmetrical medium. When TIR of light rays occur in a uniform spherical refractive medium, light will build up on the surface of the sphere and contain intensity maxima and minima along the circumference of the medium. However, the description of the geometrical picture of the

optical resonances cannot explain the intensity spectrum of the resonances, where the wavelength and the distribution of the light in the resonator require a field explanation. Since the radius of the sphere is much larger than the wavelength of the light, Lorenz-Mie scattering theory will be used for the explanation of the modes of the optical resonances.

In order to have a mathematical description of the whispering gallery modes (WGMs) of light on a microsphere, Maxwell's equations with spherical boundary conditions are introduced. The solution of the boundary conditions requires the introduction of the spherical harmonic vectorial functions with the integer indices of (l, n, m). These indices belong to the modes of light, which describe the field distribution along the radial, polar and azimuthal coordinates of the sphere. The field distribution of the sphere can be explained the spectral parameters of the optical resonances by introducing the mode spacing ($\Delta\lambda_n$) and the quality factor (Q). After this part, the coupling of light to the WGMs of a microsphere is given.

The coupling of light is described as the excitation of a light mode in a microsphere with the correct properties of the light. The universal coupling relations with amplitude and phase for the input and output light are given in order to explain the coupling. The resonance occurs by meeting certain matching conditions, where the impact parameter (b) is important. The impact parameter (b) for the microsphere is limited by the radius and the refractive index of the microsphere, where the WGMs of the light on a microsphere can be

distributed. The impact parameter (*b*) plays an important role in the methods for the coupling of light and the optical fiber half coupler (OFHC) used in the experiments.

Chapter 3 presents the numerical simulations for the WGMs in a microsphere. This chapter is divided in two parts, where the plane wave and Gaussian beam excitations are simulated. In the numerical simulations; the polar angle dependence of the resonances is investigated together with the polarization dependence. This chapter yielded to the explanation of the number of polar modes in the elastic light scattering spectra obtained in chapter 5.

Chapter 4, describes the experimental setup for the characterization of the WGMs in a spherical resonator. For having a high refractive index for the confinement of the light modes and relatively easy integration for the device applications, the material for the microsphere resonator is chosen to be silicon. The physical parameters of the silicon microspheres are characterized with the I-V characteristics, SEM microphotographs and ellipticity measurements together with the Raman spectroscopy results. After this, the optical setup for the coupling of light and excitation of WGMs are presented. In this part, the laser diode characteristics and the properties of the fiber optical setup are given. The coupling scheme with an OFHC is presented and described in detail.

Chapter 5, gives the results for the measurements and the device application schemes for the silicon microspheres. The elastic light scattering and the observation of WGMs on the silicon microspheres are presented for 0° transmission and 90° elastic

scattering. The mode structure is analyzed with mode spacing and quality factor measurements, which corresponds well with the theoretical expectations. The analysis of the WGM spectrum continues with the characterization of the WGM clusters. These clusters can either be explained by the azimuthal mode splitting due to ellipticity or the mode splitting induced by a particle.

The azimuthal modes are naturally degenerate for a perfect sphere, where they split with the introduction of the ellipticity (e) for the microsphere. Depending on the shape distortion, the observed azimuthal mode splitting can be explained for the presented spectra. On the other hand, clustering of the resonances in the WGM might also result from the particle induced mode splitting. This phenomenon can be used for another device application, where the binding of a dielectric particle induces a greater mode splitting than the splitting induced by the ellipticity of the microsphere. The clustering of the modes in the WGM spectra can be used for the particle sizing applications where the radius of the binding particle can be found.

Following the section of the spectral characterization of the WGMs, the observed asymetrical lineshapes in the spectra are also explained. The presented measurements show a Fano type lineshape for the 90° elastic light scattering. This line shape is explained by the phase relation of the WGMs with the background (BG) created by the surface imperfections and the glare spots. The Fano lineshape observed in the measurements can be used for fast switching and filtering applications.

A biosensing scheme for DNA particles is also presented, where a particle adsorbed on the microsphere creates an observable shift in the WGM spectrum. Depending on the elastic light scattering and WGM measurements together with the electro-optical properties of the silicon, an observable change in the spectrum is predicted, when a base of DNA gets adsorbed on to the surface of the microsphere.

All in all, the optical resonances, namely WGMs are receiving an increasing attention for the accurate sizing, sensing and filtering applications. Silicon as a microsphere material is promising due to its widespread usage and easy technological integration with silicon photonics. Overall, silicon as the microsphere is a promising candidate for various novel photonic applications.

BIBLIOGRAPHY

[1]   M. Crunelle, "is tthere an acoustical tradition in western architecture," in *The turning of the world*, Banff, Canada, 1993.

[2]   L. Rayleigh, "Whispering gallery modes," *Phil. Mag.,* pp. 1001-1004, 1910.

[3]   S. K. M. T. I. H. S. &. V. F. Arnold, "Shift of whispering-gallery modes in microspheres by protein adsorption.," *Optics letters,* vol. 28, no. 4, pp. 272-274, 2003.

[4]   A. A. S. a. G. G. Serpengüzel, «Excitation of resonances of microspheres on an optical fiber,» *Optics Letters,* cilt 20, no. 7, pp. 654-656, 1995.

[5]   Ş. K. Ö. L. H. D.-R. C. a. L. Y. Jiangang Zhu, "Single virus and nanoparticle size spectrometry by whispering-gallery-mode microcavities," *Optics Express,* vol. 19, no. 17, pp. 16195-16206, 2011.

[6]   Ş. K. Ö. J. Z. a. L. Y. Lina He, "Ultrasensitive detection of mode splitting in active optical microcavities," *Physical Review A,* vol. 82, pp. 053810-4, 2010.

[7]   F. A. S. &. K. D. Vollmer, "single virus detection from reactive shift of a whispering gallery mode," *Proc. Natl. Acad. Sci. USA,* pp. 20701-20704, 2008.

[8]   J. a. B. O. Ward, "WGM microresonators: sensing, lasing and fundamental optics with microspheres," *Laser Photonics rev.,* vol. 5, no. 4, pp. 553-570, 2011.

[9]   J. O. S. K. X. Y. F. L. L. H. L. C. D. R. &. Y. L. Zhu, "On-chip single nanoparticle detection and sizing by mode splitting in an ultrahigh-Q microresonator," *Nature Photonics,* vol. 4, no. 1, pp. 46-49, 2009.

[10] M. L. S. A. A. &. I. V. S. Gorodetsky, "Ultimate Q of optical microsphere resonators," *Optics Letters,* vol. 21, no. 7, pp. 453-455, 1996.

[11] M. L. P. A. D. &. I. V. S. Gorodetsky, "Rayleigh scattering in high-Q microspheres," *J. Opt. Soc. Am. B,* pp. 1051-1057, 2000.

[12] B. E. L. J. H. H. A. Little, "Analytic Theory of Coupling from Tapered Fibers and Half-Blocks into Microsphere Resonators," *Journal of Lightwave Technology,* vol. 14, pp. 704-715, 1999.

[13] V. S. M. L. Y. X. S. Ilchenko, "Pigtailing the high-Q microsphere cavity: a simple fiber coupler for optical whispering-gallery modes," *Optics Letters,* vol. 24, no. 11, pp. 723-725, 1999.

[14] J.-P. a. L. B. a. L. D. a. T. H. a. K. L. a. H. H. Laine, "Microsphere resonator mode characterization by pedestal anti-resonant reflecting waveguide coupler," *IEEE Photonics Technology Letters,* vol. 12, no. 8, pp. 1004-1006, 2000.

[15] V. a. G. M. a. I. V. Braginsky, "Quality-factor and nonlinear properties of optical whispering-gallery modes," *Physics Letters A,* vol. 137, no. 7, pp. 393-397, 1989.

[16] S. a. K. T. a. P. O. a. V. K. Spillane, "Ideality in a Fiber-Taper-Coupled Microresonator System for Application to Cavity Quantum Electrodynamics," *Physical Review Letters,* 2003.

[17] J. P. A. D. R. &. S. S. A. Barton, "Internal fields of a spherical particle illuminated by a tightly focused laser beam: focal point positioning effects at resonance," *Journal of Applied Physics,* vol. 65, pp. 2900-2906, 1989.

[18] Ş. B. T. S. A. K. A. İşçi, "Microsphere-based optical system for biosensor applications," *Biomedical Optics,* p. 180, 2004.

[19] Z. T. A. &. B. V. Chen, "Highly efficient optical coupling and transport phenomena in chains of dielectric microspheres," *Optics Letters,* vol. 31, no. 3, pp. 389-391, 2006.

[20] A. A. S. G. G. a. L. J. A. Serpengüzel, "Enhanced coupling to microsphere resonances with optical fibers," *J. Opt. Soc. Am. B,* vol. 14, no. 4, pp. 790-795, 1997.

[21] J. A. Lock, "Excitation efficiency of a morphology-dependent resonance by a focused Gaussian beam," *JOSA A,* vol. 15, pp. 2986-2994, 1998.

[22] S. B. a. K. M. M. a. B. E. Gorajoobi, "Characterization of Strongly Coupled Si-Wire Waveguides for High-Density Optical WDM and Sensing Applications," *Journal of Lightwave Technology,* vol. 31, no. 22, pp. 3469-3476, 2013.

[23] E. Yüce, *Optical Modulation and Spectroscopy with Silicon Microspheres,* Koc University, 2009.

[24] M. L. a. G. V. S. Ilchenko, "Optical microsphere resonators: optimal coupling to high- Q whispering-gallery modes," *J. Opt. Soc. Am. B,* vol. 16, pp. 147-154, 1999.

[25] E. Hecht, Optics, Addison Wesley, 2002.

[26] H. W. D. S. &. K. M. Chew, "Elastic scattering of evanescent electromagnetic waves," *Applied Optics,* vol. 18, no. 15, pp. 2679-2687, 1979.

[27] P. C. R. A. d. F. F. &. D. J. P. Chaumet, "Evanescent light scattering: The validity of the dipole approximation," *Physical Review B,* vol. 58, no. 4, p. 2310, 1998.

[28] D. S. S. V. H. J. L.-S. V. R. J. M. &. H. S. Weiss, "Splitting of high-Q Mie modes induced by light backscattering in silica microspheres," *Optics letters,* vol. 20, no. 18, pp. 1835-1837, 1995.

[29] T. B. M. J. &. M. W. Hirschfeld, "Virometer: an optical instrument for visual observation, measurement and classification of free viruses," *Journal of Histochemistry & Cytochemistry,* vol. 25, no. 7, pp. 719-723, 1977.

[30] A. C. H. J. W. &. H. R. E. Pipino, " Evanescent wave cavity ring-down spectroscopy with a total-internal-reflection minicavity," *Review of scientific instruments,* vol. 68, no. 8, pp. 2978-2989, 1997.

[31] E. Ambrose, "A surface contact microscope for the study of cell movements," *Nature,* vol. 178, no. 4543, p. 1194, 1956.

[32] D. Axelrod, "Cell-substrate contacts illuminated by total internal reflection fluorescence," *The Journal of Cell Biology,* vol. 89, no. 1, pp. 141-145, 1981.

[33] J. C. D. N. S. V. H. J. L.-S. V. R. J. M. &. H. S. Knight, "Characterizing whispering-gallery modes in microspheres by direct observation of the optical standing-wave pattern in the near field,"

Optics letters, vol. 21, no. 10, pp. 698-700, 1996.

[34] J. C. Maxwell, A treatise on electricity and magnetism, Clarendon Press, 1881.

[35] L. V. Lorenz, Œuvres scientifiques, Copenhagen: Johnson Reprint Corp., 1898.

[36] G. Mie, "Pioneering mathematical description of scattering by spheres," *Ann. Phys,* vol. 25, p. 337, 1908.

[37] H. v. Helmholtz, Handbuch der physiologischen Optik, Hamburg: Hamburg: Voss, 1909.

[38] C. F. a. H. D. R. Bohren, Absorption and scattering of light by small particles, John Wiley & Sons, 1983.

[39] A. Demir, *Elastic scattering of gaussian beams from spheres,* Istanbul: Koc University, 2005.

[40] C. a. P. A. Fabry, "Theorie et applications dune nouvelle methode de spectroscopie interferentielle," vol. 16, no. 7, 1899.

[41] A. Siegman, Lasers, Mill Valley, CA: University Science Books, 1986.

[42] P. Chylek, "Resonance structure of Mie scattering: distance between resonances," *J. Opt. Soc. Am. A,* vol. 7, no. 9, pp. 1609-1613, 1990.

[43] J. Jackson, Classical Electrodynamics, Newyork: John Wiley & Sons, 1998.

[44] M. C. G. N. R. G. C. D. Y. R. D. S. S. Ferrari, "Whispering gallery mode microresonators: Fundamentals and applications," *Rivista del Nuovo Cimento,* vol. 34, no. 7, 2011.

[45] A. Yariv, "Universal relations for coupling of optical power between microresonators and dielectric waveguides," *Electronics Letters,* vol. 36, no. 4, pp. 321-322, 2000.

[46] P. W. a. H. S. C. Barber, Light scattering by particles: Computational Methods, World Scientific, 1990.

[47] J. A. &. G. G. Lock, "Generalized Lorenz-Mie theory and applications," *Journal of Quantitative Spectroscopy & Radiative Transfer,* vol. 110, pp. 800-807, 2009.

[48] J. A. Lock, "Improved Gaussian beam-scattering algorithm," *Applied Optics,* vol. 34, pp. 559-570, 1995.

[49] S. H. a. R. Benner, "Morphology-dependent resonances associated with stimulated processes in microspheres," *J. Opt. Soc. Am. B.,* vol. 3, no. 11, pp. 1509-1514, 1986.

[50] H.-B. L. A. H. a. A. C. J. D. Eversole, "Spherical-cavity-mode assignments of optical resonances in microdroplets using elastic scattering," *J. Opt. Soc. Am. A.,* vol. 7, no. 12, pp. 2159-2168, 1990.

[51] J. P. R. C. MH. Fields, "Nonlinear optics in microspheres," in *Progress in optics*, Elsevier, 2000, pp. 1-95.

[52] J. F. D. a. A. M. Parker, "Raman Scattering by Silicon and Germanium*," *Physical Review Letters,* vol. 155, pp. 712-714, 1967.

[53] P. A. &. H. C. E. Temple, "Multiphonon Raman spectrum of silicon," *Physical Review B,* vol. 7, pp. 3685-3697, 1973.

[54] A. &. C. R. Zwick, "Multiple-order Raman scattering in crystalline and amorphous silicon," *Physical Review B,* vol. 48, pp. 6024-6032, 1993.

[55] A. K. A. &. A. U. K. Serpengüzel, "Silicon microspheres for electronic and photonic integration," *Photonics and Nanostructures-Fundamentals and Applications,* vol. 6, pp. 179-182, 2008.

[56] D. I. K. A. T. A. K. W. R. M. M. R. M. A. L. a. J. C. Garbuzov, "14xx nm DFB InGaAsP/InP pump lasers with 500 mw CW output power for WDM combining," in *Optical Fiber Communication Conference and Exhibit, OFC2002*, California, 2002.

[57] G. J. C. N. M. S. A. D. T. a. A. S. Griffel, "Morphology-dependent resonances of a microsphere–optical fiber system," *Optics Letters,* vol. 21, no. 10, pp. 695-697, 1996.

[58] L. A. K. a. I. P. G. Li, "Single-mode optical fiber tunable couplers," *Fiber Optic Components and reliability,* vol. 1580, pp. 205-215, 1992.

[59] Y. L. Y. L. R. K. &. Y. A. Xu, "Scattering-theory analysis of waveguide-resonator coupling," *Physical Review E,* vol. 62, no. 5, 2000.

[60] A. M. A. S. a. V. I. L. Maleki, "Tunable delay line with interacting whispering-gallery-mode resonators," *Optics Letters,* vol. 29, no. 6, pp. 626-628, 2004.

[61] A. M. D. S. V. I. a. L. M. A.A. Savchenkov, "Mode filtering in optical whispering gallery resonators," *Electronics Letters,* vol. 41, no. 8, pp. 495-497, 2005.

[62] S. T. C. H. A. H. J. F. a. J.-P. L. B. E. Little, "Microring Resonator Channel Dropping Filters," *Journal of Lightwave Technology,* vol. 15, no. 6, pp. 998-1005, 1997.

[63] L. Y. D. S. &. C. M. K. Mario, "Asymmetric Fano resonance and bistability for high extinction ratio, large modulation depth, and low power switching," *Optics express,* vol. 14, no. 26, pp. 12770-12781, 2006.

[64] M. M. C. &. W. M. Popovic, "Coupling-induced resonance frequency shifts in coupled dielectric multi-cavity filters," *Optics express,* vol. 14, no. 3, pp. 1208-1222, 2006.

[65] M. Z. a. A. S. Ulaş S. Gökay, "Spherical Silicon Optical Resonators: Possible Applications to Biosensing," *European Journal of Physics Special Topics,* 2014.

[66] R. C. S. H. a. P. B. Gang Chen, "Frequency splitting of degenerate spherical cavity modes: stimulated Raman scattering spectrum of deformed droplets," *Optics Letters,* vol. 16, no. 16, pp. 1269-1271, 1991.

[67] J. C. Y. K. L. D. H. &. C. R. K. Swindal, "Precession of morphology-dependent resonances in nonspherical droplets," *Optics letters,* vol. 18, pp. 191-193, 1993.

[68] T. J. Kippenberg, "Microresonators: Particle sizing by mode splitting," *Nature Photonics,* vol. 4, no. 1, pp. 9-10, 2010.

[69] X. T. a. S. A. D. Keng, "Whispering gallery micro-global positioning system for nanoparticle sizing in real time," *Applied Physics Letters,* vol. 105, p. 071105, 2014.

[70] Ş. K. Ö. J. Z. a. L. Y. Lina He, "Ultrasensitive detection of mode splitting in active optical microcavities," *Physical Review A,* vol. 82, p. 053810(4), 2010.

[71] L. A. F. a. J. B. Comunale, "Splitting of low-Q Mie resonances," *J. Opt. Soc. Am. A,* vol. 15, no. 7, pp. 1858-1866, 1998.

[72] H. T. Z. L. &. P. A. W. Lee, "Fano resonances in prism-coupled multimode square micropillar resonators," *Optics letters,* vol. 30, no. 12, pp. 1527-1529, 2005.

[73] Y. F. L. B. B. J. X. F. L. Y. &. G. Q. Xiao, "Fano resonance in whispering gallery photonic microcavities," *In Proc. of SPIE Vol,* vol. 8564, pp. 85640V-1, 2012.

[74] B.-B. Y.-F. X. C.-L. Z. Y.-C. L. X.-F. J. Y.-L. C. Y. L. a. Q. G. Li, "Experimental observation of Fano resonance in a single whispering-gallery microresonator," *Applied Physics Letters,* vol. 98, no. 2, p. 021116, 2011.

[75] S. W. Y. W. J. &. W. A. Nic Chormaic, "Fano Resonances and Electromagnetically Induced Absorption and Transparency-like Effects in Single Silica Microspheres," *Laser Science- Optical Society of America,* p. p. JWA47, 2010.

[76] S. Fan, "Sharp asymmetric line shapes in side-coupled waveguide-cavity systems," *Applied Physics Letters,* vol. 80, no. 6, pp. 908-910, 2002.

[77] H. a. G. Z. Quan, "Simulation of whispering-gallery-mode resonance shifts for optical miniature biosensors," *Journal of Quantitative Spectroscopy & Radiative Transfer,* vol. 93, pp. 231-243, 2005.

[78] M. S. Y. E. G. O. S. A. Murib, "Polarization behavior of elastic scattering from a silicon microsphere coupled to an optical fiber," *Photon. Research 2,* no. 45, 2014.

[79] O. M. a. A. Lagendijk, "Method for broadband spectroscopy of light transport through opaque scattering media," *Optics Letters,* vol. 34, no. 4, pp. 395-397, 2009.

[80] S. a. B. R. L. Schiller, "High resolution spectroscopy of whispering gallery modes in large dielectric spheres," *Opt. Lett.,* vol. 16, p. 1138, 1991.

APPENDIX

Autocorrelation and signal analysis for the elastic light scattering

The following section presents the autocorrelation function (ACF) analysis of the elastic light scattering spectrum. The ACF can be used for the determination of the mode spacing, which may yield to particle sizing applications [79], [65]. The analysis is performed with a custom autocorrelation function (ACF) with the backgrounds of the elastic light scattering intensities subtracted. In the ACF spectrum, the polar mode spacing of the silicon microsphere is clearly visible. Additionally, the observed spectra were measured at 90°, which is expected to have 4 polar mode families in a mode spacing. This behavior is also met in the ACF spectra with the correlation of the 0° and 90° elastic light scattering.
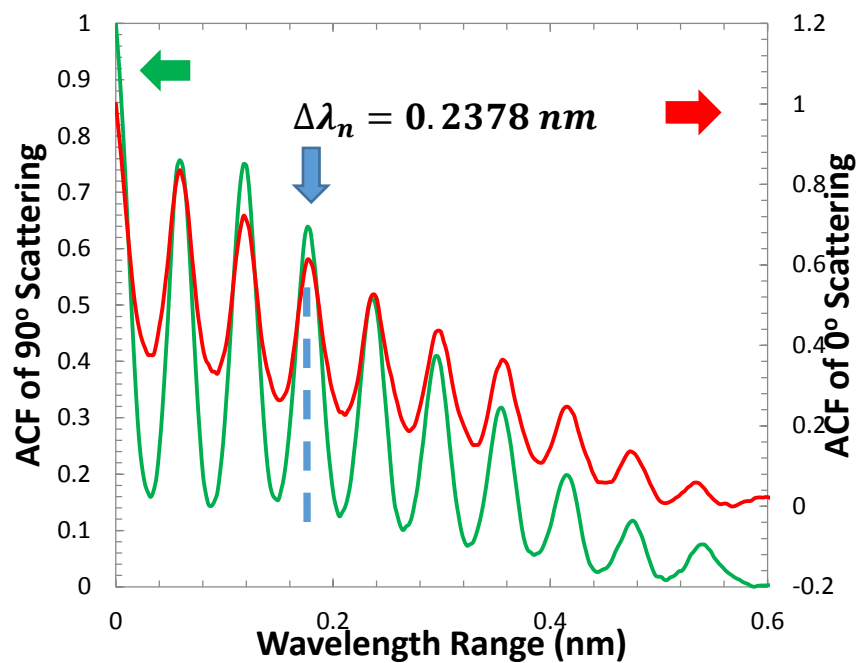
Figure A.1: ACF analysis of the spectrum presented in Fig. 5.1.

CURRICULUM VITAE

2009 – 2014 PhD: "Elastic Light Scattering and Optoelectronic Response of Spherical Microresonators"
Physics Department, Koç University
Supervised by Prof. Ali Serpengüzel – will be submitted in spring 2014
Funded by Koç University, GSSE Institute
My thesis investigates the properties and novel applications of the spherical microresonators in opto-electronics. I have successfully participated in a TUBITAK project with an international collaboration during my PhD studies. We have worked in the fields of:
- Liquid crystal based optical modulators
- Spherical solar cells
- Applications of high quality factor microspheres in optical devices

Preparation of the thesis is on progress and it is expected to be completed with the end of spring semester, 2014.

2006 – 2009 MSc: "Studies on melt-textured growth $YBa_2Cu_3O_{7-x}$ superconductors"
Physics Department, Ege University
Supervised by Assoc. Dr. Mustafa Tepe
Funded by Ege University BAP projects division
My thesis investigates the electrical and magnetic properties of bulk $YBa_2Cu_3O_{7-x}$ ceramic materials for high temperature superconductivity. My research topic included the following fields:
- Production of superconducting high critical temperature bulk composite crystalline materials
- Optimization of electric and magnetically properties by Y211 doping. Thesis project was accepted by Ege University with Master of Science degree in September 2009.

2002 – 2006 BSc degree obtained from Physics department, Bilkent University
I was accepted with a full scholarship for undergraduate studies to the Bilkent university physics department.

Modules covered included basic physics and mathematics courses, classical mechanics, electromagnetic theory, quantum theory and mechanics, solid state physics, statistical physics and nuclear physics.
Senior year dissertation - "Theory of 2D harmonic oscillators and Landau level wavefunctions" was done with Prof. Dr. Mehmet Özgür Öktel and was accepted in May 2006.

1998 – 2002   High School Degree was obtained from İzmir Atatürk Lisesi (İAL) with the top rank and was honored with an escutcheon on the historical recording board of the school.

RESEARCH EXPERIENCE
2011 – 2012   Corporation with Kyosemi Company from Japan
Successful optical and electronic characterization of the spherical silicon solar cells (SphelarOne) and their application in microresonator studies.
2009 – 2011   Researcher for the TUBITAK project of EEEAG106E215
Successful collaboration with CNR institute of Rome, TUBITAK and Koç University for the project titled as "Optical resonance studies of liquid crystal embedded glass microspheres" under the supervision of Prof. Dr. Ali Serpengüzel and Dr. Romeo Becherelli. A proceeding paper titled as "Silicon microsphere based filtering applications for near-infrared optical fiber based telecommunications" was published for the Optical MEMS and Nanophotonics (OMN) international conference in 2011.

- Novel Approaches – developed a conceptual opto-electronic device based on the interaction of the light with microspheres embedded in liquid crystal medium predicted by Serpenguzel and Becherelli. Elastic light scattering spectra and resonance modulation measurements were done on the concept.
- Research project delivery – delivered the results on time within the budget while regularly reviewing the project plans and results with the supervisors.
- Collaboration – Performed characterization measurements for the project, helped developing the concept with Huzeyfe Yilmaz, MSc degree research colleague from the physics department, Koc University. Paid a visit to Dr. Becherelli in CNR institute of Rome for the final review of the project.

2008 – 2009   One semester exchange program
I was accepted as a researcher by Leiden Institute of Physics, Netherlands in the framework of Erasmus Student Mobility Project. I worked in the magnetic and superconducting materials research division of Kamerlingh Onnes laboratory under the supervision of Prof. Dr. Jan Aarts and successfully completed the fabrication and investigation of Nb/FeMn thin film spin switches as well as obtaining magnetization measurements for bulk YBCO samples. Following are the list of topics I worked on:

- Novel Approaches – studied the physical properties of the magnetic domains in thin film geometries and focused on spin-orbit interaction theory of ferromagnetic materials. Manufactured Nb/FeMn thin film structures and performed characterization with SQUID based magnetic properties measurement systems.

- Research project delivery – delivered a formal report to the department in 7 months. During this time I was funded by several bursaries from the union of IAL graduates, Turkish Businessmen association of Netherlands and by the Leiden Institute.

- Collaboration - successfully worked with an international research environment.

RESEARCH TECHNIQUES
2009 – 2013

- Establishments of free space alignment, telecom and fiber optic measurement setups
- Tunable IR diode, pulsed Nd:YAG, gas discharge and solid state laser operation
- Excitation, fluorescence and Raman spectrometry measurements
- Elastic light scattering and applications of whispering gallery mode (WGM) resonators
- Measurement device communication and LabView user interface developments

2006   – 2009

- Operation of tubular furnace and temperature cycle systems for bulk ceramic material preparation

- Establishment of low temperature electromagnetic measurement systems
- Magnetization, magnetic susceptibility and critical temperature measurements in SQUID based MPMS and PPMS systems.
- Metallic thin film fabrication in UHV sputtering systems and pattern writing with e-beam lithography.